LRH-1/NR5A2 Activation in Immune Cells from Individuals with Type 1 Diabetes Mellitus Mitigates Inflammation via Immunometabolic Reprogramming and Enhanced Human Islet Function in Mice

Cobo-Vuilleumier N[1], Rodríguez-Fernandez S[2*], López-Noriega L[1*], Lorenzo PI[1], Franco JM[1], Lachaud CC[1], Martin Vazquez E[1], Araujo Legido R[1,3], Dorronsoro A[1], López-Férnandez-Sobrino R[1], Fernádez-Santos B, Salas-Lloret D[4], van Overbeek N[4], Ramos-Rodriguez M[5], Mateo-Rodríguez C[6], Hidalgo L.[6], Nano R[7], Arroba, AI[8], Campos Caro A[8], Vertegaal ACO[4], Martin Montalvo A[1], Martín F[1,3], Aguilar-Diosdado M[8], Piemonti L[7], Pasquali L[5], González Prieto R[1,9], García Sánchez MI[10], Martínez-Brocca MA[6$], Vives-Pi M[2$], Gauthier BR[1,3,11,#]

[1]Andalusian Center of Molecular Biology and Regenerative Medicine-CABIMER, Junta de Andalucía-University of Pablo de Olavide-University of Seville-CSIC, Seville, Spain
[2]Immunology Department, Germans Trias i Pujol Research Institute, Autonomous University of Barcelona, Badalona, Spain
[3]Centro de Investigación Biomédica en Red de Diabetes y Enfermedades Metabólicas Asociadas (CIBERDEM), Madrid, Spain
[4]Cell and Chemical Biology, Leiden University Medical Centre, Einthovenweg 20, 2333ZC Leiden, The Netherlands
[5]Pompeu Fabra University, Barcelona, Spain
[6]Department of Endocrinology and Nutrition. University Hospital Virgen Macarena, Sevilla, Spain
[7]Diabetes Research Institute, IRCCS Ospedale San Raffaele, Milan, Italy
[8]Department of Endocrinology and Nutrition. University Hospital Puerta del Mar, Institute of Research and Innovation in Biomedical Sciences of Cádiz (INiBICA). University of Cádiz (UCA), Spain.
[9]Department of Cell Biology, Faculty of Biology, University of Sevilla, Spain
[10]Biobank of the Andalusian Public Health System, Node Hospital Virgen Macarena, Sevilla, Spain
[11]Lead contact

[*]These authors contributed equally to this work
[$]These senior authors contributed equally to this work.

[*]Correspondence: Benoit R. Gauthier (ORCID: 0000-0001-8146-7486)
CABIMER: Andalusian Center of Molecular Biology and Regenerative Medicine Avenida Américo Vespucio, 24 41092 Sevilla, Spain
Tel: +34 954 467 468
Fax: +34 954 461 664
Email: benoit.gauthier@cabimer.es

SUMMARY

The intricate etiology of type 1 diabetes mellitus (T1DM), marked by a detrimental cross-talk between the immune system and insulin-producing β-cells, has impeded effective disease-modifying therapies. The discovery that pharmacological activation of the nuclear receptor LRH-1/NR5A2 can reverse hyperglycemia in mouse models of T1DM by attenuating the autoimmune attack coupled to β-cell survival/regeneration, prompted us to investigate whether immune tolerization could be achieved in individuals with T1DM by LRH-1/NR5A2 activation as well as improving islet function/survival after xenotransplantation in mice. Pharmacological activation of LRH-1/NR5A2 induced a coordinated immunometabolic reprogramming of T1DM macrophages and dendritic cells, shifting them from a pro- to an anti-inflammatory/tolerogenic phenotype. Regulatory T-cells were also expanded resulting in the impediment of cytotoxic T-cell proliferation. LRH-1/NR5A2 activation enhanced human islet engraftment and function in hyperglycemic immunocompetent mice. These findings demonstrate the feasibility of re-establishing immune tolerance within a pro-inflammatory environment, opening a new therapeutic venue for T1DM.

INTRODUCTION

Contrary to most autoimmune diseases, Type 1 Diabetes Mellitus (T1DM) is gender impartial and stands out as one of the most prevalent chronic pediatric illnesses affecting 1.75 million individuals under the age of 20 years (https://diabetesatlas.org/atlas/t1d-index-2022/). A recent study estimated that in 2021 there were 355 900 new cases of T1DM in children and adolescents worldwide of which only 56% were diagnosed. This number is projected to increase to 476 700 by 2050 [1]. Classically, T1DM has been considered a T-cell-mediated autoimmune disease caused by a disruption in the balance between T-regulatory cells (Tregs) and T-effector cells (Teffs; $CD4^+$ and $CD8^+$ cytotoxic T-cells) that respond to islet-associated self-antigens [2,3]. This breakdown in immune homeostasis or 'tolerance' leads to β-cell destruction resulting in insulin deficiency, hyperglycemia, and the lifelong necessity for insulin supplementation in afflicted individuals [4]. Based on this immune origin, several immunosuppressive therapies have been developed and their safety demonstrated in clinical trials. One of these, teplizumab (anti-CD3 derivative) was recently approved by the Food and Drug Administration (FDA) and delays the development of T1DM in individuals 'at-risk' by 2 years. While representing a significant breakthrough, the limited effectiveness timeframe underscores the disease's more complex root cause [5,6]. Considering the latter, the contribution of β-cells in the pathogenesis of T1DM has gained momentum, as evidenced by the expression of several T1DM susceptible gene variants in the β-cells. These gene variants modulate pro-inflammatory signals and cause vulnerability to endoplasmic reticulum (ER) and oxidative stress, triggering cell dysfunction and apoptosis. Due to the highly vascularized islet microenvironment, β-cell stress signals reach circulating immune cells, initiating a cross-talk. This cross-talk may ultimately result in the destruction of β-cells and is further influenced by other genetic and environmental factors [7-9]. Therefore new effective disease-modifying therapies (DMT) for T1DM, should aim to

resolve this detrimental dialogue by simultaneously targeting both immune and islet cells [10].

Nuclear receptors (NRs) play pivotal roles in a wide range of physiological and pathological processes [11]. They regulate metabolic pathways that control cellular energy balance, survival, and adaptability to the environment. NRs are also crucial for whole-organism functions such as development, metabolism, reproduction, immune response, and tissue regeneration. The fact that NRs activities can be controlled by ligands has made them attractive targets for drug development, with potential therapeutic applications [12,13]. One such NR is the liver receptor homolog 1 (LRH-1 *a.k.a.* NR5A2), which has emerged as a promising drug target for diseases like diabetes, pancreatic cancer, non-alcoholic fatty liver disease, and metabolic syndrome. [14-20]. Our previous work provided an early proof-of-concept that pharmacological activation of LRH-1/NR5A2 using a small chemical agonist (BL001) could therapeutically impede the progression of hyperglycemia in 2 mouse models (NOD and RIP-B7.1) of T1DM, validating the benefits of targeting this NR [21]. BL001 coordinated *in vivo* the resolution, rather than the suppression, of the autoimmune attack, by increasing the number of anti-inflammatory M2 while decreasing the number of pro-inflammatory M1 macrophages, and concomitantly increasing the number of IDO^+ tolerogenic dendritic cells and Tregs. In parallel, BL001 stimulated β-cell regeneration via trans-differentiation and improved cell survival, the latter involving the PTGS2/PGE_2/PTGER1 signalling cascade [21-23].

Given the strong disease-modifying properties of LRH-1/NR5A2 activation in mouse models of T1DM, and aiming for the clinical applicability of this strategy, herein we expanded our studies to primary immune cells obtained from individuals with T1DM. Our endpoint was to define the molecular mode of action of LRH-1/NR5A2 agonistic activation in T1DM cells, which is especially relevant considering that the diabetic milieu impedes the anti-inflammatory characteristics of both human macrophages and dendritic

cells [24-26]. Furthermore, we sought to determine whether LRH-1/NR5A2 activation could facilitate long-term human islet engraftment and function in immunocompetent hyperglycemic mice.

RESULTS

LRH-1/NR5A2 activation reduces the expression of pro-inflammatory markers on monocyte-derived macrophages and dendritic cells isolated from healthy and T1DM individuals

Peripheral blood mononuclear cells (PBMCs) were isolated from blood samples procured from healthy and T1DM individuals, with an average age of 33 and 37 years, respectively, a body mass index (BMI) of approximately 23-24, and equal sex representation (**Table 1**). We focus on adults with long-established T1DM as this population has been the most challenging to refrain from disease progression with novel immunomodulatory drug therapies. $CD14^+$ monocytes were purified from PBMCs and derived either into naïve/primed ($MDM1_0$) or pro-inflammatory macrophages (MDM1) and immature (iDC) or mature dendritic cells (mDC) [27,28]. Cell viability was greater than 90% for all groups. Due to the restricted number of cells isolated from each blood sample, individual preparation of macrophages and DCs was used in specific subsets of experiments (flow cytometry, cytokine profiling, omics, etc.). We initially profiled cell surface markers associated with either a pro- or anti-inflammatory/tolerogenic phenotype in the presence or absence of the pharmacological activation of LRH-1/NR5A2 using the small chemical agonist BL001. LRH-1/NR5A2 activation significantly reduced the levels of the prototypical pro-inflammatory macrophage surface marker CD80 in MDM1 obtained from both healthy and T1DM donors (**Figure 1A**). Expression levels of CD14, which facilitates LPS binding to Toll-like receptor 4 (TLR4) and promotes an M1 phenotype [29], decreased in both $MDM1_0$ and MDM1 from individuals with T1DM, but not those of healthy donors, after BL001 treatment (**Figure 1B**). In parallel, BL001 increased the expression of the anti-inflammatory cell surface marker CD206 in $MDM1_0$

of both healthy and T1DM individuals, while the anti-inflammatory CD209 was only significantly increased in MDM1 obtained from healthy but not in those of T1DM individuals (**Figure 1C and D**). In contrast, expression levels of CD86, CD163, and CD200R remained relatively constant in all the experimental groups (**Figure S1A-C**). Next, we measured the expression of several cell surface markers involved in antigen presentation and T-cell activation which are associated with a proinflammatory mDC phenotype. Agonistic activation of LRH-1/NR5A2 did not alter the expression of proinflammatory cell surface markers on iDCs from either healthy or T1DM donors but increased the expression of CD36 - implicated in the clearance of apoptotic cells, inhibiting antigen presentation and DC maturation- exclusively in T1DM iDCs (**Figure 1E and Figure S1E-M**). In contrast, CXCR4, and CD54 expression levels were blunted in BL001-treated T1DM mDCs (**Figure 1F and G**), while healthy BL001-treated mDCs exhibited reduced levels of CXCR4 and CD25 as compared to untreated cells (**Figure 1G and H**). These findings collectively suggest that the pharmacological activation of LRH-1/NR5A2 not only reduces the expression of key pro-inflammatory cell surface markers in both T1DM MDM1 (CD80 and CD14) and mDCs (CXCR4 and CD54) but also imposes an anti-inflammatory phenotype on naïve $MDM1_0$ and iDCs, further limiting the recruitment/activation of additional MDM1 and mDCs. Furthermore, these results also highlight that cells isolated from T1DM individuals respond differently to BL001 as compared to cells procured from healthy individuals, likely as a consequence of molecular alterations imposed by the long-term disease state [24-26]. In contrast, alterations in the expression of MDM and DC surface markers by BL001 were sex independent.

LRH-1/NR5A2 activation suppresses pro-inflammatory cytokine secretion from MDMs and DCs isolated from individuals with T1DM

The reduction of pro-inflammatory surface markers in both MDMs and DCs prompted us to assess whether the pharmacological activation of LRH-1/NR5A2 would also modulate their cytokine secretion profile, further favouring an anti-inflammatory environment. We

focused on immune cells isolated from individuals with T1DM as future DMT will target specifically this population. For the analysis of the cytokine secretion profile, we used a commercial antibody array that covers a total of 80 different cytokines. We found that BL001 treatment of T1DM $MDM1_0$ significantly increased the secretion of angiogenin (ANG) and CCL4 (*a.k.a* macrophage inflammatory protein-1β, MIP-1β) (**Figure 2A).** Angiogenin is associated with an anti-inflammatory and wound-healing response in macrophage [30]. CCL4 is recognized as a chemokine-attracting T-cells, including Tregs [31], but has recently also been shown to promote angiogenesis via angiopoietin-2 in oral squamous cell carcinoma [32]. In T1DM MDM1, BL001 treatment significantly altered the secretion of 6 cytokines (**Figure 2B**). Noteworthy is the decreased secretion of CXCL6 and CCL13, both of which stimulate the chemotaxis of M1 macrophages [33]. Additionally, BL001 reduced the secretion from T1DM donors of TNFSF14, a member of the TNF family that triggers the NF-κB signalling pathway leading to the induction of various chemokines including CXCL6 [34]. The pharmacological activation of LRH1/NR5A2 also diminished the secretion of macrophage migration inhibitor factor (MIF) and TNFRSF11 (*a.k.a.* osteoprotegerin, OPG), two cytokines known for their pro-inflammatory activity. Deficiencies in these factors have been shown to induce an LPS-hyporesponsive phenotype [35,36]. Conversely, the secretion of CCL7, a chemokine that attracts M1 but also M2 macrophages [33], was found to increase in response to BL001 treatment.

Activation of LRH-1/NR5A2 in T1DM iDCs significantly decreased the secretion of several members of the CC-chemokine subfamily (CCL2, CCL24, and CCL26), all of which play roles in various inflammatory diseases by recruiting leukocytes to sites of inflammation (**Figure 2C**) [37]. Correlating with this decline in chemokine secretion, FGF9, which is known to increase expression of pro-inflammatory chemokines like CCL2 in the central nervous system [38] exhibited lower levels in T1DM iDCs treated with BL001. In parallel, the release of the pro-inflammatory cytokines IL-6, LIF (member of the IL-6 family), IL-7, and IL-8 was reduced in BL001-treated T1DM iDC (**Figure 2C**). Secretion

levels of leptin, HGF, IGFBP1, FLT3 ligand, BDNF, and PDGFBB were also decreased in BL001-treated iDCs (**Figure 2C**). Leptin is known for its role in driving DCs maturation, leading to Th1 priming, while the blockade of HGF is associated with the resolution of the pro-inflammatory phase, considered a critical step in restoring tissue homeostasis [39,40]. Elevated serum IGFBP1 levels have been observed in individuals with T1DM. The Flt3/Flt3L signalling pathway, as well as BDNF, have been linked to several autoimmune diseases [41-43]. Similarly, PDGF-BB has been identified as a key mediator of inflammation and fibrosis induced by CXCL4 in the rare autoimmune disorder systemic sclerosis [44].

BL001-treated T1DM mDCs also exhibited a reduction in the secretion of IL-7 and IL-8 (**Figure 2D**), which may be particularly relevant since two independent studies have demonstrated that blocking the IL-7 receptor could reverse autoimmune diabetes in NOD mice by repressing effector T-cells (Teffs) [45,46]. Furthermore, high circulating levels of IL-8 have been associated with poor metabolic control in adolescents with T1DM [47]. In addition, BL001 treatment decreased the secretion of the key cytokine IL-1B, which determines the inflammatory milieu during T1DM, as well as IGFBP2 and IGFBP3, which are normally elevated in individuals with T1DM (**Figure 2D**) [41,48].

Taken together, our results indicate that LRH-1/NR5A2 activation reduces the secretion of several pro-inflammatory cytokines/chemokines in MDM1, mDCs, and iDCs, thereby attenuating the propagation of pro-inflammatory cells. Moreover, LRH-1/NR5A2 activation increases the secretion of pro-angiogenic cytokines ANG and CCL4 in $MDM1_0$ while simultaneously decreasing the secretion of the anti-angiogenic factor HGF in iDCs. This intricate response underscores the multifaceted role of LRH1/NR5A2 activation in shaping the immune microenvironment towards an anti-inflammatory and regenerative state.

LRH-1/NR5A2 agonistic activation attenuates the pro-inflammatory genetic signature of T1DM MDMs

To investigate the molecular consequences resulting from LRH-1/NR5A2 pharmacological activation and understand its immunomodulatory effects at the cellular level, we conducted RNAseq analysis on T1DM-isolated MDMs. Since the transcriptome profiles of either untreated $MDM1_0$ or MDM1 obtained from healthy individuals diverged from those of T1DM individuals (**Figure 3A**), our focused was on assessing the impact of BL001 on T1DM MDM, as future clinical trials are expected to target this specific group. Remarkably, $MDM1_0$ displayed a greater number of differentially expressed genes (DEGs) than MDM1 upon BL001 treatment (1376 versus 671) (**Figure S2 and Figure 3B and E**). Gene set enrichment analysis (GSEA) revealed that common DEGs shared by $MDM1_0$ and MDM1 subpopulations clustered into KEGG pathways predominantly related to hematopoietic cell lineage commitment, cholesterol, and fatty acid metabolism. In contrast, DEGs specific to $MDM1_0$ clustered into cell cycle, genome dynamic, and RNA metabolism, whereas genes altered only in MDM1 clustered into inflammatory pathways and apoptosis (**Figure S2**). Accordingly, functional enrichment analysis of DEGs in BL001-treated $MDM1_0$ compared to untreated cells revealed the activation of enriched pathways for ribosomes, sphingolipid metabolism as well as autophagy. In contrast, cancer-related pathways (gastric cancer, p53, and transcription. misregulation in cancer) and the cell cycle pathway were suppressed as evidenced by decreased expression of numerous histone-encoding genes (**Figure 3C and D**). Of particular interest was the up-regulation of DDIT4 and GRB10, both involved in the inhibition of mTOR (**Figure 3D, brown arrows**) [49,50]. DDIT4 conveys the anti-inflammatory effects of IL-10 on pro-inflammatory M1 macrophages through the inhibition of mTOR and the activation of autophagy/mitophagy resulting in the clearance of damaged mitochondria, lower levels of reactive oxygen species and blunted NLRP3 inflammasome activation [50]. In line with these effects, transcript levels of NLRP3 and its downstream target IL1B were reduced in BL001-treated $MDM1_0$ (**Figure 3D, blue**

arrows). Collectively, these results suggest that BL001 coerces $MDM1_0$ into an anti-inflammatory and non-proliferative phenotype that secretes higher levels of regenerative factors (**Figure 2A**). Notably, in BL001 treated T1DM MDM1, lysosome was the only positively enriched pathway, while a myriad of pro-inflammatory-associated pathways such as the chemokine signalling pathway, cytokine-cytokine receptor interaction, and Toll-like receptor signalling, were suppressed (**Figure 3F**). It is worth noting that lysosomal dysfunction has been linked to impair autophagy flux contributing to M1 macrophage polarization under diabetic conditions [51]. This suggests that the activation of the lysosomal pathway, which includes the ACP5 gene that was significantly up-regulated in BL001-treated T1DM MDM1 (**Figure 3E and G, red arrows**), may be involved in suppressing the pro-inflammatory phenotype. Primary murine macrophages lacking ACP5 display a pro-inflammatory phenotype with increased secretion of IL-1B and IL12 [52]. These cytokines, along with the inflammasome sensor NLRP3, the TLR4, and NF-κB signalling pathways were all decreased in BL001-treated T1DM MDM1 (**Figure 3F and G, purple arrows**). Consistent with a shift towards an anti-inflammatory and pro-regenerative phenotype, the most statistically significant up-regulated gene was GPNMB/osteoactivin for which the soluble form was shown to promote angiogenesis (**Figure 3E, green arrow**) [53].

LRH-1/NR5A2 activation inhibits a subset of mitochondrial proteins in T1DM $MDM1_0$ and MDM1

To map global changes including post-transcriptional/translational alterations induced by LRH-1/NR5A2 activation, we determined the proteomic profile of T1DM $MDM1_0$ and MDM1 treated or not with BL001. This analysis revealed the presence of 188 differentially expressed proteins (DEPs) (87 up- and 91 down-downregulated proteins, $p<0.05$) out of a total of 1890 quantifiable proteins in $MDM1_0$ (**Figure 4A, Table S1 and S2**). Similarly, in T1DM MDM1 we identified 287 DEPs (151 up- and 136 down-downregulated proteins, $p<0.05$) out of 1953 quantifiable proteins (**Figure 4B, Table S3**

and S4). The relatively limited number of DEPs identified posed a challenge to the analysis of enriched pathways. Consequently, we opted to investigate the protein-protein interaction (PPI) network among these DEPs. Consistent with the enrichment of the aminoacyl-tRNA biosynthesis and ribosome pathways observed in GSEA (**Figure 3C**), several interacting proteins among the up-regulated DEPs in BL001-treated T1DM $MDM1_0$ were related to translation initiation and tRNA synthesis (**Figure 4C, grey shaded area**). Remarkably, a PPI cluster of mitochondrial proteins was identified in the down-regulated DEPs of BL001-treated $MDM1_0$ which was not identified by the GSEA (**Figure 4D**, **pink shaded area**). Next, we performed an integrative analysis of the transcriptome and proteome to highlight common DEGs and DEPs. This analysis revealed 14 up- and 16-down regulated transcripts/proteins shared by both omics (**Figure 4E, green circles and F**). Of particular interest, the transferrin receptor (TFRC), common to both omics, was the most up-regulated DEPs in BL001-treated $MDM1_0$ (**Figure 4A, C and F purple arrow**). Deletion of this receptor in murine macrophages was shown to promote a M1-like polarization driven by IFNγ, suggesting that its increased expression may sway an anti-inflammatory phenotype [54]. Similarly, BST2 (*a.k.a.* Tetherin) was the most down-regulated DEPs, consistent with a significant decrease in transcript levels in BL001-treated $MDM1_0$ (**Figure 4A, D and F green arrow**). Tetherin is an anti-viral agent that induces pro-inflammatory gene expression via NF-κB [55], indicating that its suppression will likely impede $MDM1_0$ activation towards an MDM1 phenotype.

In contrast to the GSEA in BL001-treated MDM1, which revealed lysosome as the only activated pathway (**Figure 3F**), most of the up-regulated DEPs interacting with each other, clustered in global gene transcription/translation, including RNA polymerase (POLR2A), translation initiation factors (EIF4A1, the second most up-regulated DEP) and ribosomal subunits (RPL8, RPL7A, etc.) (**Figure 4G, French beige shaded area**). The most up-regulated DEP, SPTBN1, was shown to inhibit inflammatory responses and

hepatocarcinogenesis in hepatocellular carcinoma via down-regulation of the NF-κB signalling pathway, which was also suppressed in GSEA of T1DM MDM1 [56] (**Figure 4B and G, black arrow and Figure 3F**). Significantly, CD14 exhibited the strongest down-regulation among DEPs in BL001-treated MDM1, aligning with the flow cytometry results and providing robust evidence of BL001´s potent anti-inflammatory effect (**Figure 4B, H and J, red arrow and Figure 1B**) [57,58]. This conclusion is substantiated by the observed decrease in proteins associated with the proteasome, for which inhibition results in a conversion to an anti-inflammatory phenotype (**Figure 4H, blue shaded area**) [59]. Similar to $MDM1_0$, several mitochondrial proteins were repressed in BL001-treated MDM1, evidencing that LRH-1/NR5A2 activation affects mitochondrial function (**Figure 4H, pink shaded area**) [20,60]. We then compared and contrasted the transcriptome and proteome of BL001-treated MDM1 and found that 4 up- and 6 down-regulated genes were common to both omic approaches (**Figure 4I, red circles and J**). CD14 was the most down-regulated gene/protein, emphasizing that BL001 blocks the initial proinflammatory signalling receptor to prevent further stimulation by LPS (**Figure 4J, red arrow**). Of particular interest, ATP-citrate lyase (ACLY) was also consistently decreased in both omics and resulted in lower levels of Acetyl CoA in BL001-treated MDM1s (**Figure 4J, orange arrow and K**). LPS promotes histone acetylation via increased ACLY activity and higher levels of Acetyl CoA, which licences the transcription of pro-inflammatory genes such as IL1B [61]. Our data may suggest that lower levels of ACLY and Acetyl CoA could result in decreased histone acetylation, leading to the repression of the pro-inflammatory gene response.

LRH-1/NR5A2 activation drives mitohormesis to enforce a pro-inflammatory tolerant state in T1DM MDM1

A hallmark of LPS-induced pro-inflammatory reprogramming of macrophages is a time-dependent shift in ATP production from oxidative phosphorylation (OXPHOS) to glycolysis [62]. As a consequence of these metabolic changes and as a feedback

mechanism to prevent cell impairment, macrophages trigger a stress response called mitohormesis [63]. This response, which includes a cross-talk between the nuclei and the mitochondria, attempts to re-establish mitochondrial homeostasis and induce an LPS tolerance state, thereby avoiding an exacerbated and perpetual pro-inflammatory response. In this context, several hydroxyestrogens were recently shown to induce mitohormesis in macrophages, enforcing an LPS-immuno-resistant phenotype [64]. This highlights mitohormesis as an unprecedented and controversial therapeutic target to counteract inflammation. As LRH-1/NR5A2 pharmacological activation suppressed the expression of mitochondrial proteins in both $MDM1_0$ and MDM1, we wondered whether BL001 could induce mitohormesis in macrophages. To validate this premise, we assessed the mitochondrial metabolic flux in T1DM MDMs. The addition of LPS to $MDM1_0$ to generate MDM1 significantly reduced the basal oxygen consumption rate (OCR) as compared to non-LPS-treated $MDM1_0$, consistent with the switch from OXPHOS to glycolysis to support a pro-inflammatory phenotype (**Figure 5A and B**). BL001 further decreased the basal OCR in MDM1 as well as in $MDM1_0$ even to lower levels than those found before the LPS treatment (**Figure 5A and B**). In parallel, transcript and protein levels of ATF4, the key activator of mitohormesis, as well as transcript levels of its downstream target GDF15 were significantly increased (**Figure 5C-E**). In contrast, the expression of both IL1B and NLRP3 was blunted in BL001-treated T1DM MDM1 (**Figure 5F and G**). Taken together, these results suggest that LRH-1/NR5A2 agonistic activation likely triggers mitohormesis to enforce a pro-inflammatory immune-paralyzed state. We then assessed whether this immune-paralyzed state could impact stimulation of naïve $CD4^+$ and $CD8^+$ T-cell proliferation, which is typically triggered by professional antigen-presenting cells such as macrophages and DCs [65,66]. $CD4^+$, but not $CD8^+$ T-cell proliferation was dampened by BL001-treated MDM1 derived from T1DM individuals, indicating that BL001 reprogramming of MDM1 partly inhibits T-cell proliferation (**Figure 5H and I**). MDMs from healthy individuals did not impede T-cell

expansion, independent of BL001 treatment further evidencing fundamental differences between healthy and T1DM derived macrophages (**Figure 5H and I**).

NR5A2 promotes mitochondrial turnover favouring tolerization of T1DM mDCs

To explore the potential anti-inflammatory effect of LRH-1/NR5A2 pharmacological activation conveyed onto DCs, we conducted bulk RNAseq analysis. Similar to MDMs, we observed differences in the transcriptome profiles between untreated iDCs and mDCs from healthy individuals and those with T1DM (**Figure 6A**). Therefore, we focused on mapping the molecular effects of BL001 on T1DM DCs, with the rationale that forthcoming clinical trials would likely target this group rather than healthy individuals. BL001 induced alterations in the expression of a limited number of genes in T1DM iDCs, with no significant changes detected in KEGG pathways (**Figure 6B**) while a broader array of genes was altered in T1DM mDCs (**Figure 6C**). Functional enrichment analysis of BL001-treated T1DM mDCs revealed the activation of some pathways, including the lysosomal pathway, and suppression of others such as 'viral protein interaction with cytokine and cytokine receptor' and 'cytokine-cytokine receptor interaction', both of which were also decreased in T1DM MDM1 treated with BL001 (**Figure 6C black arrows, E and Figure 3F**). Additionally, pathways related to phagosome, oxidative phosphorylation, and PPAR signalling were also activated by BL001 in T1DM mDCs (**Figure 6E**). Notably, all these pathways, along with the lysosome pathway, are known to play crucial roles in the tolerogenicity of DCs [67]. Supporting this premise, several key tolerogenic genes such as VEGFA and B, TGFB1 and 2, PTGS2, and CD36 were all significantly up-regulated in BL001-treated mDCs (**Figure 6F**). The most activated pathway in BL001-treated T1DM mDCs was OXPHOS (**Figure 6D red arrow and E**). Similar to macrophages, a switch from OXPHOS towards glycolysis is the main trigger activating mDCs [68]. Thus, stimulation of OXPHOS via increased fatty acid oxidation (FAO) driven by the PPAR signalling pathway (also among the top activated pathways- **Figure 6D blue arrow**) may induce an anti-inflammatory and tolerizing phenotype in

mDCs. To ascertain this hypothesis, we assessed the mitochondrial metabolic flux of DCs isolated from T1DM individuals treated with or without BL001 and palmitate. Similar to MDM, maturation/activation of iDCs resulted in decreased basal OCR (**Figure 7A and B**). However, the addition of BL001 alone or together with palmitate did not increase/potentiate basal OCR as compared to untreated mDCs (**Figure 7A and B**). Subsequent analysis revealed upregulation of the lysosomal and phagosome pathways in BL001-treated mDCs, along with genes associated with increased acidification and hydrolase activity (**Figure 6D and E**). These findings suggest a potential induction of mitophagy to eliminate dysfunctional mitochondria, coinciding with the generation of new functional mitochondria as indicated by the increased expression of mitochondrial-related genes (**Figure 6E**). To corroborate this premise, mitochondrial mass and membrane potential were assessed by flow cytometry using the probes MitoTracker Green (binding covalently to mitochondrial proteins, thus providing an assessment of mass) and MitoTracker Red (taken up by polarized mitochondria, thus gauging function) [69]. BL001-treated T1DM mDCs displayed a reduced proportion of cells with non-functional mitochondria (MitoTracker Green^{High} and MitoTracker Red^{low}) compared to untreated cells. This outcome supports the premise that LRH-1/NR5A2 activation in mDCs could facilitate mitochondrial turnover, which may be associate with the emergence of a tolerogenic phenotype (**Figure 7C**). In line with this, BL001 impeded mDCs-mediated stimulation of autologous CD4^{+} and CD8^{+} T-cell proliferation in individuals with T1DM (**Figure 7D and E**). Furthermore, BL001-treated T1DM iDCs also displayed reduced capacity to stimulate CD8^{+} T-cell proliferation, which correlated with increased levels of CD36 in these cells (**Figure 7E and Figure 1H**). Moreover, both CD4^{+} and CD8^{+} T-cell proliferation were decreased when exposed to healthy mDCs treated with BL001 (**Figure 7D and E**). Such cells also displayed reduced expression of the activation marker CD25, which was previously shown to prime CD4^{+} T-cells [70] (**Figure 1F**). Taken together, our results suggest that BL001 induces the reprogramming of mDCs

towards tolDCs via mitochondria turnover, resulting in reduced proliferation of T-effector cells.

BL001 promotes the expansion of a $CD4^+/CD25^+/FoxP3^+$ Tregs subpopulation in individuals with T1DM which inhibits $CD8^+$ T-cell proliferation

In view of the anti-inflammatory benefits imparted by BL001 on both MDM1 and mDCs from T1DM donors, we pondered whether BL001 could also sway the expansion of $FoxP3^+$ Tregs, which enforce peripheral self-tolerance, counteracting self-immunity. $CD4^+$ T-cells from both healthy and T1DM individuals were activated using CD3 and CD28 antibodies for 24 hours before the addition of BL001. The Treg subpopulation was then determined by flow cytometry using CD45, CD4, CD25, and FoxP3 markers. BL001 treatment significantly increased the percentage of $CD4^+/CD25^+/FoxP3^+$ Tregs in T1DM individuals but not in healthy donors (**Figure 8A**). Although $CD4^+$ T-cells proliferation showed no significant changes, $CD8^+$ T-cells proliferation was decreased by BL001 treatment of T-cells, correlating with the increased $CD4^+/CD25^+/FoxP3^+$ Tregs subpopulation (**Figure 8B and C**).

BL001 improves human islet graft survival and function in STZ-treated immune-competent mice

We have demonstrated that pharmacological activation of LRH-1/NR5A2 confers immunomodulatory benefits on human macrophages, DCs, and Tregs. The current results extend our previous findings on BL001 to promote tolerogenesis and enhance islet cell survival in the RIP-B7.1 and streptozotocin-induced DM mouse models [21]. Given these common benefits on both murine and human immune cells, we next proceeded to evaluate whether BL001-mediated immune tolerance could attenuate graft rejection and improve the survival and function of human islets transplanted into hyperglycemic and immunocompetent C57BL/6j mice. To this end, we performed suboptimal human islet transplantations (750 human islet equivalents; IEQ) under the

kidney capsule of mice rendered diabetic with a single high dose of streptozotocin (STZ). One week after transplantation, mice were treated or not with BL001. The rationale for using suboptimal amounts of IEQ was to examine whether any potential improvements in human islet cell survival and insulin secretion could lead to improved glycemia, endowed by the BL001 treatment. Three independent experiments were performed with 3 diferent donors, two of which the BL001 regimen was for up to 4 weeks and 1 for up to 8 weeks (**Figure 9A and L**). Although hyperglycemia persisted at either 4 and 8 weeks, blood glucose levels were lower in transplanted mice treated with BL001 for up to 8 weeks correlating with a higher survival rate as compared to vehicle treated mice at either 4 or 6 weeks, time at which all mice had to be euthanized due to pre-defined health criteria (**Figure 9B, C, M and N**). Although not statistically significant, transplanted mice treated for 4 weeks with BL001 displayed a mild improvement in glucose tolerance as compared to vehicle mice **Figure 9D and E).** Human C-peptide was detected in BL001-treated mice, but not in vehicle-treated mice, at 4- and 8 weeks post-treatment, confirming some functionality of the transplanted human islet (**Figure 9F and O**). In contrast, mouse C-peptide blood levels were marginally discernable in either BL001- or vehicle-STZ-treated mice, as compared to untreated mice, 4 and 8 weeks post-treatment (**Figure 9G and P**). Both BL001- and vehicle-treated mice sacrificed at 4-weeks retained human islet xenotransplants with a similar number of INS and GCG expressing cells as well as $CD4^+$ T-cell infiltration (**Figure 9H-K**). The 8-week extended BL001-treatment preserved both the β- and α-cell mass along with $CD4^+$ T-cell infiltration in xenotransplants correlating with improved glycemia while vehicle-treated mice that were sacrificed at 6 weeks (due to pre-defined health criteria) exhibited a significantly lower number of INS expressing cells and a higher number of GCG expressing cells as compared to BL001-treated mice (**Figure 9Q-T**). Taken together, these results indicate that BL001 favours the survival, engraftment, and function of a marginal mass of human islets in STZ-treated immunocompetent C57BL/6J.

DISCUSSION

Despite substantial research and development efforts across both academia and pharmaceutical sectors, a long-term pharmacological solution that can significantly reverse hyperglycemia in T1DM has yet to be discovered. The complexity of T1DM highlights the urgent need for a fundamental paradigm shift in our approach to understanding the disease´s intricate mechanisms, which involves a dynamic interaction between the immune system and pancreatic cells [10]. This 'symphony' underscoring the pathogenesis of T1DM[71], requires a conductor/target to orchestrate a coordinated resolution of the autoimmune attack/proinflammatory process, rather than suppression, leading to β-cell regeneration/survival [10]. Herein, using MDMs, DCs, and T-cells isolated from individuals with established T1DM and a combination of cell surface marker analysis, omics profiling, and functional studies, we demonstrate that the pharmacological activation of LRH-1/NR5A2 resolves the pro-inflammatory environment by: 1) suppressing the pro-inflammatory M1-like phenotype of MDM1 while maintaining $MDM1_0$ in a naïve state through mitohormesis, 2) fostering a reprogramming of mDCs towards tolDCs by promoting mitochondrial turnover, thereby reducing $CD4^+$ and $CD8^+$ T-cells proliferation and 3) enhancing the expansion of $CD4^+/CD25^+/FoxP3^+$ Tregs subpopulation, leading to diminished $CD8^+$ T-cell proliferation. In parallel, our study demonstrates that the activation of LRH-1/NR5A2 can enhance the engraftment and function of human islets transplanted into diabetic immunocompetent mice. As such, we argue that LRH-1/NR5A2 fulfills all criteria of a 'symphony conductor' orchestrating resolution of the autoimmune attack coupled to improved islet cell survival and potential regeneration [10,21]. Given these promising results, it is conceivable that NR therapeutic targets like LRH-1/NR5A2 could also be effective in addressing other autoimmune diseases. To the best of our knowledge, our study is one of the first to demonstrate that a pharmacological compound not only imparts anti-inflammatory properties to fully activated MDM1s and mDCs of individuals with T1DM but also promotes human engraftment and function in immunocompetent C57/BL6j, likely via tolerization as we

previously demonstrated [21]. Most studies have primarily concentrated on non-fully mature DCs, evaluating the effects of compounds such as 1α,25-Dihydroxyvitamin D3 on DCs maturation and activation, but none have investigated their potential to transform fully mature DCs isolated from individuals with T1DM into a tolerogenic phenotype [72,73]. Similarly, most human islet transplantation survival and functional studies have been carried out in immunodeficient mice to prevent rejection [74]. Herein, we selected the STZ-treated C57/BL6j mouse model with the specific intention of expanding on our previous findings on BL001 tolerizing a pro-inflammatory environment, key for the sustained engraftment and long-term functionality of human islets [21]. Consequently, our findings hold significant implications for human clinical studies, since reversing T1DM will require addressing the chronic pro-inflammatory/autoimmune responses, which are primarily driven by macrophages and dendritic cells activated by islet self-antigens. These cells are pivotal in triggering T-cell proliferation and the subsequent β-cell destruction [75].

Our findings also emphasize the cell context-dependent nature of the genetic alterations and phenotypic outcomes induced by LRH-1/NR5A2 pharmacological activation. This is evidenced by the disparity in the molecular pathways regulated in BL001-treated MDM1s and mDCs, with many pathways suppressed in MDM1 but activated in mDCs. In MDM1s, LRH-1/NR5A2 activation suppressed multiple pathways implicated in inflammatory responses (15 out of 20), correlating with decreased expression of key cell surface markers such as CD14 and CD80, and reduced secretion of pro-inflammatory cytokines and chemokines. Interestingly, BL001 did not induce expression of M2-associated cell surface markers such as CD206, CD209, and CD200R suggesting that the action of LRH-1/NR5A2 activation is to neutralize/incapacitate the pro-inflammatory M1 phenotype rather than promoting a transition towards an M2-like phenotype. Accordingly, although BL001-treated T1DM $MDM1_0$ harbored higher levels of CD206 at the cell surface, both transcript and protein levels were decreased (**Figure 4F**, CD206 *a.k.a.* MRC1), substantiating the premise that LRH-1/NR5A2 does not promote an M2-like

phenotype but rather suppresses a M1 phenotype. The concept of M1 incapacitation is further evidenced by the instatement of an immune-paralyzed phenotype via mitohormesis induced by BL001, which is consistent with previous studies reporting that LPS/IFNγ-mediated mitochondrial shutdown prevents IL-4 polarization of M1 towards an M2 phenotype [76]. Additionally, BL001´s anti-inflammatory properties are highlighted by the inhibition of multiple enriched pathways related to inflammatory responses (systemic lupus erythematosus, influenza A, Epstein-Barr virus, among others), as well as pathways involved in either cell cycle or cellular senescence in BL001-treated $MDM1_0$. These molecular events translated to the inhibition of $CD4^+$ T-cells proliferation indicative of a resorbed Teff-mediated cell destruction. Notably, the mitohormesis-related factor GDF15, which was increased in BL001-treated T1DM MDM1s, was shown to be expressed in a subset of macrophages and to promote muscle regeneration [77]. Additionally, GDF15 expression was lower in T1DM pancreas and its exogenous administration prevented insulitis progression in NOD mice and protected isolated human pancreatic islets. [78]. Concurrently, pharmacological activation of LRH-1/NR5A2 led to upregulated expression of angiogenin and CCL4 in $MDM1_0$ from T1DM individuals. Both angiogenin and CCL4 induce angiogenesis, which is essential for supporting the formation of new blood vessels necessary for the delivery of nutrients and oxygen to growing tissues [32,79]. Taken together, these data emphasize the premise that BL001 favours a regenerative environment through increased expression of GDF15, angiogenin, and CCL4 from MDMs [10,21]. In this context, we have previously shown that CCL4 serum levels were increased in BL001-treated hyperglycemic RIP-B7.1 mice correlating with immune coupled α- to β-cell trans-differentiation [21]. Angiogenin was also shown to cleave tRNAs, through its ribonuclease activity, thereby transiently inhibiting translation in cells under stress conditions to quickly adapt to their new environment [80,81]. Accordingly, the top two activated enriched pathways in BL001-treated T1DM $MDM1_0$ were aminoacyl-tRNA biosynthesis and ribosome, evidencing an autocrine effect of angiogenin to alleviate stress-induced molecular reprogramming.

Pharmacological activation of LRH-1/NR5A2 reprogrammed T1DM mDCs towards a tolerogenic-like phenotype. This is evidenced by the activation of key molecular pathways inducing tolerance, such as OXPHOS, PPAR signalling, lysosome, and phagosome, as well as a specific subset of tolerogenic-associated genes, including PTGS2. Previously, we demonstrated that PTGS2 and its product, prostaglandin E_2, endow a tolerogenic phenotype to DCs after efferocytosis and prevent cytokine-induced apoptosis in BL001-treated islet β-cell [22,23,82]. Consistent with a shift towards a tolerogenic phenotype, levels of several cell surface markers associated with mDCs (CXCR4 and CD54) were decreased, as did the secretion of IL-7 in cells treated with BL001. Of high relevance, a recent clinical trial assessing the efficacy of the humanized anti–IL-7R monoclonal antibody RN168 in subjects with T1DM revealed a significant decline in $CD4^+$ and $CD8^+$ effector and central memory T-cells along with an increase in Tregs [83]. BL001 treatment of mDCs from T1Dm donors, similarly suppressed the proliferation of both $CD4^+$ and $CD8^+$ T-cells suggesting a potential role of IL-7 in this process. This premise is further substantiated by the decreased levels of IL-7 in BL001-treated iDCs, which also impeded $CD8^+$ T-cell expansion. Contrary to our initial hypothesis and based on RNAseq data revealing BL001-mediated activation of the PPAR and OXPHOS pathways, with no net differences in mitochondrial respiration experiments, we advocate that the phenotypic switch induced by LRH-1/NR5A2 activation is likely mediated by enhanced mitochondrial turnover. The latter is supported by a decreased number of mDCs with dysfunctional mitochondria and previous studies demonstrating that mitophagy/autophagy contributes to maintaining an anti-inflammatory phenotype [84].

Tregs play a key role in sustaining peripheral tolerance, and their dysfunction has been reported in individuals with T1DM [85,86]. Consequently, clinical trials involving autologous Tregs reinfusion following *in vitro* expansion, have shown a transient increase in these

cells, correlating with enhanced islet survival and C-peptide levels, rendering Tregs as a promising cell-based therapy for T1DM [87,88]. Nevertheless, these cells were found to be short-lived in transfused patients, and a subsequent clinical trial that combined Tregs with IL-2 to improve survival, also increased cytotoxic T-cells [87,89]. Herein, we demonstrate that BL001 stimulates the expansion of the $CD25^+/FoxP3^+$ Tregs subpopulation within the T-cell population, with a concomitant decrease in cytotoxic $CD8^+$ T-cell proliferation, offering an appealing pharmacological alternative to cell therapy.

Consistent with its anti-inflammatory properties observed in both mice [21] and human immune cells, we demonstrate that the therapeutic administration of BL001 to hyperglycemic immunocompetent mice xenotransplanted with human islets favours graft implantation and functionality. While our prior work demonstrated that short-term BL001 treatment could protect transplanted human islets in mice against rejection, long-term engraftment, and function, as evaluated by circulating human C-peptide was not assessed in that study [21]. Our findings have substantial implications for future immunomodulatory therapies in combination with the transplantation of either human islets or induced pluripotent stem cell (hIPSC)-derived islet-like organoids, which are also susceptible to immune rejection. Current strategies to avoid graft rejection encompass cell encapsulation and/or aggressive immunosuppressant regimens, often resulting in secondary complications such as kidney failure [90-92]. Alternatively, hIPSC-derived islet-like organoids are being genetically modified to successfully evade the autoimmune attack in pre-clinical mouse models [93,94]. Nonetheless, these approaches have yet to reach ethical approval for clinical trials. Pharmacological activation of LRH-1/NR5A2 could circumvent these caveats encountered by cell therapy by attenuating the pro-inflammatory environment- without suppressing the general immune system- while increasing β-cell survival and performance [22,23].

Overall, our findings introduce a new dimension in T1DM therapies, where the pharmacological activation of LRH-1/NR5A2 instructs the genetic and metabolic reprogramming of human monocyte-derived macrophages, dendritic cells, and T-cells from individuals with T1DM to support an anti-inflammatory and regenerative environment. This resolution of the autoimmune attack also promotes islet survival and function (**Figure 10**).

Limitations of the study

Although our study was intentionally targeted to adults with long-standing T1DM, the immunomodulatory benefits of BL001 should also be assessed in either young or older individuals who have recently been diagnosed with T1DM in which the strong autoimmune attack may be more resilient to any drug treatment. While the mode of action of LRH-1/NR5A2 agonistic activation has been elucidated in distinct populations of macrophages and dendritic cells as well as its impact on T-cells *in vitro*, the net physiological outcome endowed by BL001 in a more complex milieu comprised of several interacting immune cell types along with islets have yet to be evaluated. Furthermore, whether regenerative factors secreted by immune cells exposed to BL001 will promote human β-cell regeneration remains to be assessed. Modelling T1DM *in vitro* will address these limitations [95].

STAR METHODS

Detailed methods are provided in the online version of this article and include the following:

- KEY RESOURCES TABLE
- RESOURCES AVAILABILITY
    - Lead contact
    - Materials availability
    - Data and code availability

- EXPERIMENTAL MODEL AND SUBJECT DETAILS
    - Ethical approval
    - Clinical samples
    - Human islet procuration
    - Mice

- METHOD DETAILS
    - Peripheral blood mononuclear cell (PBMC) and monocyte isolation
    - Monocyte-derived macrophages (MDMs) and dendritic cells (DCs)
    - $CD4^+$ T-cell isolation
    - BL001 treatment
    - Flow Cytometry
    - Cytokine profiling
    - Autologous T Cell Proliferation Assay
    - Transcriptome profiling
    - Proteomic profiling
    - Acetyl Coenzyme A measurement
    - RNA extraction and quantitative real-time PCR
    - Western blot
    - Mitochondrial bioenergetic and fitness
    - Xenotransplantation
    - Immunofluorescence analyses
    - Morphometric analyses

- QUANTIFICATION AND STATISTICAL ANALYSIS

SUPPLEMENTAL INFORMATION

Supplemental information can be found online at XXX

ACKNOWLEDGMENTS

We thank Dr. Maria José Quintero from the Cytometry Core Facility and the team from the Genomic Core Facility of CABIMER as well as Pedro Antonio Soriano Fernandez and Noelia García Rodríguez for their excellent technical support. Special thanks to all donors and to the Biobank Node of the Hospital Virgen Macarena (Biobanco del Sistema Sanitario Público de Andalucía) which is part of the Spanish National biobanks Network (PT20/00069) supported by Instituto Carlos III and FEDER funds. We acknowledge the support of the Basic Experimentation in Diabetes study group of the Spanish Association of Diabetes as well as positive discussion through the Consolidated Research Group 2021 SGR 00002, AGAUR, Generalitat de Catalunya. Human islets for research were provided, in part, by the Alberta Diabetes Institute IsletCore at the University of Alberta in Edmonton (www.bcell.org/adi-isletcore) with the assistance of the Human Organ Procurement and Exchange (HOPE) program, Trillium Gift of Life Network (TGLN), and other Canadian organ procurement organizations. Islet isolation was approved by the Human Research Ethics Board at the University of Alberta (Pro00013094). All donors' families gave informed consent for the use of pancreatic tissue in research. The authors are supported by grants from the Consejería de Salud y Consumo, Fundación Pública Andaluza Progreso y Salud, Junta de Andalucía (PI-0727-2010 and PI-0001-2020 to B.R.G), the Consejería de Economía, Innovación y Ciencia (P10.CTS.6359 to B.R.G and DOC_00652, FSE and Lema: Andalucía moves with Europe to L.L.N.), the Ministerio de Ciencia E Innovación (BFU2017-83588-P, PID2021-123083NB-I00 financed by MCIN/AEI/10.13039/501100011033 and by FEDER, UE to B.R.G,), The DiabetesCERO Foundation (B.R.G.), the Spanish Diabetes Society and the Juvenile Diabetes Research Foundation (17-2013-372, 2-SRA-2019-837-S-B, 3-SRA-2023-1307-S-B to B.R.G.). P.A.S.F. is contracted through an action funded by the EU-NextGenerationEU, and the Recovery, Transformation and Resilience Plan (SE/INV/0008/2022) granted to the Consejería de Empleo, Formación y Trabajo Autónomo of the Junta de Andalucía in the 2022 call of the Investigo Program, Mechanism for Recovery and Resilience.

AUTHOR CONTRIBUTIONS

N.C.V., R.G-P., A.M.M., M.A.G.S., M.A.M.B., M.V.P., and B.R.G. were involved in research design. N.C.V., S.R.F., D.S-L., L.L.N., B.F.S., P.I.L, J.F.M., A.D., E.M.V., R.A.L., C.C.L., N.v.O., C.M.R., L.H., R.L.F.S., A.C.O.V., A.M.M., A.I.A., A.C.C. L.A.F. and F.M. contributed to conducting experiments. N.C.V., S.R.F., L.L.N., P.I.L, J.F.M., A.D., C.C.L., M.R.R, L.P., M.V.P., R.G-P, and B.R.G contributed to data analysis. R.N., L.P., and M.A.D. supplied human samples and reagents. N.C.V., and B.R.G. wrote the manuscript. All authors commented on the manuscript. B.R.G. is the guarantor of this work and, as such, has full access to all the data in the study and takes responsibility for the integrity of the data and the accuracy of the data analysis.

DECLARATION OF INTERESTS

Two patents (WO 2011 144725 A2 and WO 2016 156531 A1) related to BL001 have been published of which B.R.G and N.C.V. are inventors. These patents have been licenced to ARIDDAD Therapeutics, a Biotech spinoff co-founded by B.R.G. and N.C.V. along with European business partners. M.V.-P. holds a patent that relates to immunotherapy for T1D and is co-founder and SEO of Ahead Therapeutics S.L., which aims at the clinical translation of immunotherapies for the treatment of autoimmune diseases. The other authors declare no competing interests related to the current study.

INCLUSION AND DIVERSITY

We support an inclusive and equitable conduct of research.

STAR METHODS

RESOURCES AVAILABILITY

Lead contact

Further information and requests for resources and reagents should be directed to and will be fulfilled by the lead contact, Benoit R. Gauthier (benoit.gauthier@cabimer.es).

Materials availability

All unique/stable reagents generated herein are available from the lead contact upon request.

Data and code availability

Data

All data reported in this paper will be shared by the lead contact upon request.

Mass spectrometry data

The mass spectrometry proteomics data have been deposited to the ProteomeXchange Consortium via the PRIDE [96] partner repository with the dataset identifier PXD045222.

RNAseq data

The RNAseq data have been deposited to the NCBI BioProject and can be retrieved with the project ID number PRJNA1017470.

Code

This paper does not report original code.

EXPERIMENTAL MODEL AND SUBJECT DETAILS

Ethical approval

The Clinical/Investigation Ethical Committees of the Hospital Germans Trias i Pujol and the University Hospital Virgen Macarena and Rocio approved all experiments with human islets and blood-derived cells (PI-19-142, GAUTHIER-201306722 and 2057-N-22) and have been conducted following the principles outlined in the Declaration of Helsinki for human research. Mouse experimentations were approved by the Andalusian Ministry of Agriculture, Farming, Fish and Sustainable Development (08/07/2019/120). Animal studies were performed in compliance with the ARRIVE guidelines [97].

Clinical samples

Samples of 30-50 mL peripheral blood were collected by venipuncture from individuals with T1DM (68) and control healthy subjects (37) in BD Vacutainer Sodium Heparin tubes (BD Biosciences, San Jose, CA, USA). Inclusion criteria were: 20-55 years of age, body mass index 18-30 kg/m^2 and an evolution of the disease longer than 5 years. Exclusion criteria were: being under immunosuppressive or anti-inflammatory treatment, or undergoing pregnancy or breastfeeding. Patients were informed of the procedure and signed a written consent prior to blood extraction. The collection and processing of personal and clinical data from included subjects were limited to those data necessary

to achieve the objectives of the study, and the data collected was processed with adequate precautions to ensure confidentiality and compliance with applicable data privacy protection laws and regulations.

Human islet procuration

Human islets were either obtained from the Alberta Diabetes Institute IsletCore Laboratory (CA) (*n=2* donors) or from ECIT-San Raffaele Scientific Institute, Milan (IT) (*n=1* donor). Human islet preparations were washed, handpicked and subsequently maintained in CMRL-1066 (ThermoFisher Scientific) containing 5.6 mM glucose, and supplemented with 10% FCS, 100 Units/ml penicillin, 100 µg/ml streptomycin and 100 µg/ml gentamycin (all purchased from Sigma-Aldrich).

Mice

C57BL/6J mice were purchased from Janvier Labs (Saint-Berthevin Cedex, FR). Mice were housed in ventilated plastic cages under a 12-h light/dark cycle and given food and water *ad libitum*.

METHODS DETAILS

Peripheral blood mononuclear cell (PBMC) and monocyte isolation

Peripheral blood mononuclear cells (PBMCs) were isolated using either Ficoll Paque or Histopaque 1077 density gradient centrifugation. The PBMC layer was extracted and washed with PBS. Cells were resuspended in PBS, 2% FBS, 1mM EDTA buffer and monocytes were then isolated using the magnetic EasySep Human $CD14^+$ Selection kit (STEMCELL Technologies, Vancouver, BC, Canada) following the manufacturer's instructions. When the purity of CD14 marker in the selected fraction was greater that 90%, monocytes were cultured in 24-well plates (Labclinics, Barcelona, Spain) at a concentration of 10^6 cells/ml in either X-VIVO 15 media (Lonza, Basel, Switzerland) or RPMI 1640 media (ThermoFisher Scientific), both supplemented with 2% male AB

human serum (Biowest Nuaillé, France), 100 IU/ml penicillin (Sigma-Aldrich and Normon SA, Madrid, Spain), 100 µg/ml streptomycin (Sigma-Aldrich, Madrid, Spain). The negatively selected fraction of PBMCs was cryopreserved in FBS (ThermoFisher Scientific) with 10% dimethylsulfoxide (Sigma-Aldrich, Saint Louis, MO, USA) at a 10-20X10^6 cells/ml and stored for later use.

Monocyte-derived macrophages (MDMs) and dendritic cells (DCs)

Purified $CD14^+$ monocytes were derived into either macrophages (MDM) or dendritic cells (DCs). For MDM, cells were treated with 1,000 IU/ml rhGM-CSF (Prospec, Rehovot, Israel) for 3 days to generate naïve/primed $MDM1_0$ and subsequently with a cocktail containing 20ng/ml of INFγ (Immunotools, Friesoythe, Germany) and 10ng/ml of LPS (Sigma-Aldrich) to promote the pro-inflammatory MDM1 phenotype. Alternatively, monocytes were treated with 1000 IU/ml rhIL-4 and 1000 IU/ml rhGM-CSF (Prospec, Rehovot, Israel) for 6 days to obtain DCs. Media and cytokine stimuli were replenished at day 4. Dendritic cells were either cultured with 20 µg/ml human insulin (Sigma-Aldrich) to obtain immature DCs (iDCs) or adding a cytokine cocktail (CC) consisting of tumor necrosis factor (TNF)α (1000 IU/ml, Immunotools, Friesoythe, Germany), IL1β (2000 IU/ml, Immunotools) and Prostaglandin E2 (PGE2, 1 µM, Cayman Chemical, Ann Arbor, MI, USA) to obtain mature DCs (mDCs). All derived cell types were maintained at 37ºC in the presence of 5% CO_2.

$CD4^+$ T-cell isolation

The $CD4^+$ T-cell subpopulation was isolated from the $CD14^-$ fraction of PBMCs using the Easysep human $CD4^+$ T-cell isolation kit (Stemcell Technology) as per the instructions of the manufacturer. $CD4^+$ T-cells were cultured in RPMI 1640 media (ThermoFisher Scientific), supplemented with 2% male AB human serum (Biowest Nuaillé, France), 100 IU/ml penicillin (Sigma-Aldrich and Normon SA, Madrid, Spain), 100 µg/ml streptomycin (Sigma-Aldrich, Madrid, Spain). Subsequently, $CD4^+$ T-cells were activated using the

TransAct reagent (Milteny) for 24h before a single dose of 10 μM BL001 was added to the culture media.

BL001 treatment

Subsequent to the differentiation of monocytes into $MDM1_0$, MDM1, iDCs and mDCs 3 consecutive doses of 10 μM BL001 was added to the culture media; 0, 24 hours and 30 minutes prior to cell analysis or processing.

Flow Cytometry

Subpopulations of immune cells were characterized by flow cytometry (FACSCalibur and FACSAria I, BD Biosciences, Madrid, Spain), using either Zombie Violet 421 (Biolegend) or 7aad (BD Biosciences) for viability assessment and the following antibodies for 1) MDMs phenotyping: CD14 APC/FITC, CD80 PE, CD86 APC, CD163 PE-Vio615/BV421, CD200R PE, CD206 FITC/BV711, and CD209 FITC and 2) DCs phenotyping: CD11c APC, CD25 PE, CD86 FITC, HLA class I FITC, HLA class II FITC, CD14 PE and CD40 APC, CD36 APCCy7, TIM4 APC, αvβ5 integrin PE, CD54 PECy7, CXCR4 APCCy7, CCR2 APC, DC-SIGN-APC, PD-L1 PECy7 and CCR7 PECy7 (Key Resources Table). Regulatory T cells were evaluated using the REAfinity™ Treg Phenotyping Kit (Key Resources Table). Data were analyzed using either the FlowJo V9 (Tree Star) or the FCS Express softwares (De Novo Software, Pasadena, USA).

Cytokine profiling

Media was collected from MDMs and DCs, treated or not with BL001, and analyzed using the RayBiotech Human Cytokine Array C5 that interrogates 80 cytokines simultaneously (RayBiotech, Norcross, USA). Membranes were scanned and analyzed using the ImageJ/Fiji software. Results were then normalized using the internal controls of the membranes, and the relative signal intensity are represented.

Autologous T Cell Proliferation Assays

Immune cells cultured in each condition were co-cultured with autologous T lymphocytes to determine their capacity to induce T cell proliferation. Briefly, PBMCs from the same donor were thawed to be stained with the CellTrace Violet (CTV) or CFSE Cell Proliferation kit (ThermoFisher Scientific) following the manufacturer's instructions. After staining, cells were suspended in either RPMI 1640 or X-VIVO 15 complete media at a final concentration of 10^6 cells/ml, and 100,000 cells were plated in 96-well round bottom plates (Labclinics). Stained and activated PBMCs were co-cultured with either MDMs, DCs or $CD4^+$ T-cells subject to the various experimental conditions at a 10:1 or 2:1 ratio (10^5 PBMCs:10^4 DCs; $2x10^4$ PBMCs: 10^4 MDMs; $2x10^4$ PBMCs: 10^4 $CD4^+$ T-cells) in triplicates. After up to 6 days of co-culture in the incubator at 37 ºC and 5% CO2, cells were washed with 150 µL PBS per well at 400×g for 5 minutes and incubated for 20 minutes at 4 ºC with a staining mix containing CD3 PE, CD4 APC/Viogreen and CD8 FITC/PerCP-Cy5.5 staining and 7-AAD/Zombie Violet 421. Cells were then washed in PBS and T-cell proliferation was analyzed by flow cytometry. Data were analyzed using the FlowJo software (Tree Star Inc.).

Transcriptome profiling

Total RNA was isolated from human primary immune cells using the RNeasy Plus Micro Kit (Qiagen). RNA integrity number (RIN) values were evaluated using Bioanalyzer® 2100 (pico assay) and their profiles were accepted for preparing libraries for NGS (RIN >8.40). RNA-seq libraries were performed by the Genomic Facility at CABIMER, using the kit Illumina Stranded TOTAL RNA preparation RIBO-ZERO PLUS and sequenced on a NovaSeq 6000 platform with an average of 30 million reads per sample. Reads were mapped and quantify using Salmon (version 1.5.0) with default parameters to the human transcriptome (assembly GRCh38) downloaded from GENCODE genome with default parameters. Differential expression was analysed using Deseq2 using a paired

sample design. Gene set enrichment analysis was performed using clusterProfiler (version 4.0).

Proteomic profiling

Monocyte derived macrophages were lysed in 8 M urea/10 mM HEPES (pH 8.0). Samples were then supplemented with 1 mM Dithiothreitol (DDT) and incubated 30 min at RT at which point 5 mM chloroacetamide (CAA) was added and further incubated for 30 min at RT. Finally, samples were supplemented with 5 mM DTT and incubated for another 30 min at RT. Five hundred ng of Lys-C (Wako) was added to the samples and incubate for 5 h. Subsequently, three volumes of 50 mM ABC were added to dilute the urea to a final concentration of 2M. A second round of digestion with 500 ng of Trypsin (Promega) was performed overnight. Resulting peptides were desalted with C18 StageTips [98] and analyzed by label-free quantitative mass spectrometry-based proteomics using a Q-Exactive Orbitrap mass spectrometer (Thermo Scientific, Germany) equipped with an EASY-nano liquid chromatography 1000 system (Proxeon, Odense, Denmark). The Q-Exactive was coupled to a fritted fused silica capillary (25 cm L x 75 µm ID x 360 µm OD, CoAnn Technologies, Richland, US) in-house packed with 1.9 µm C18 beads (Dr. Maisch, cat:r119.aq, Ammerburch-Entringen, Germany). Peptides were separated by liquid chromatography using a 2h gradient from 2% to 95% solvent B (water/acetonitrile/formic acid at a ratio of 20/80/0.1) and followed by 0 % acetonitrile in 0.1% formic acid for chromatography column re-conditioning. The mass spectrometer was operated in positive polarity mode at 2.3 kV with the capillary heated to 250 °C. Data-dependent acquisition mode with a top 10 method was used to automatically switch between full-scan MS and MS/MS scans. Full scan MS spectra were acquired at a resolution of 70,000, an automatic gain control (AGC) target value of 3×10^6, and a scan range of 400–1,400 m/z. Precursors were fragmented by Higher-Collisional Dissociation (HCD) with a normalized collision energy of 25. Tandem mass spectra (MS/MS) were recorded with a resolution of 17,500 and an AGC target value of

1×10^5. Precursor ion masses of scanned ions were subsequently dynamically excluded from MS/MS analysis for 60 sec and only precursors with a charge state of 2-6 triggered MS/MS events. Maximum injection times for MS and MS/MS were 20 and 60 ms, respectively.

Mass spectrometry RAW files was analized using MaxQuant (v2.1.3.0) [99] . Search was performed against an in-silico digested UniProt reference proteome for Homo sapiens including canonical and isoform sequences (29th August 2022). Database searches were performed according to standard settings with the following modifications: Digestion with Trypsin/P was used, allowing 3 missed cleavages. Oxidation (M), acetyl (protein N-term) were allowed as variable modifications with a maximum number of 3. Label-Free Quantification (LFQ) was enabled, not allowing Fast LFQ. Matching between runs was enabled with a match time window of 0.7 min and an alignment time window of 20 min.

Output from MaxQuant Data were exported and processed for statistical analysis in Perseus [100]. LFQ intensity values were log2 transformed and potential contaminant and proteins either identify by site or only reverse peptides were removed. Samples were grouped in experimental categories and proteins not identified in every replicate in at least one condition were removed. Missing values were imputed using normally distributed values with 0.3 width and 1.8 down shift separately for each column. After imputation results were exported into in MS Excel and paired t-test were performed. Volcano plots were constructed for data visualization using the VolcaNoseR web [101] (https://huygens.science.uva.nl/VolcaNoseR2/). We explored the protein-protein interaction (PPI) network (PPI) among differentially expressed proteins using the online search tool for the retrieval of interacting genes/proteins (STRING v11) that comprise a database of known and predicted protein-protein interactions [102]. Networks were then

visualized in the Cytoscape software (version 3.9.1), using the yfile circular layout algorithm [103].

Acetyl Coenzyme A measurement

MDM1, treated or not with BL001, were washed in PBS and then lysed in 1M Perchloric acid. The lysate was centrifuged at 10,000g for 10 min at 4ºC. The deproteinized supernatant was neutralized with potassium bicarbonate and the neutral pH confirmed with Whatman® indicator papers. The Acetyl CoA content was then determined using the Acetyl coenzyme A assay kit as per the instructions of the manufacturer (Sigma-Aldrich). An Acetyl-CoA standard curve was plotted in the range of 0–100 pmol. Fluorescence was measured using a Varioskan Flash spectrophotometer. For normalization by protein content, the protein pellets were solubilized first in 0.2 N NaOH and then solubilized in a buffer containing 7M Urea, 2M ThioUrea, Tris 50mM ph 8.8, as previously described [104]. The protein content was determined using the Quick Start Bradford Protein assay (Biorad). Acetyl CoA content was then normalized to protein content.

Mitochondrial bioenergetic and fitness

Mitochondrial bioenergetics of MDMs and DCs were measured using the Seahorse XF Cell Mito Stress Test Kit and the XF24 Extracellular Flux Analyzer (Agilent), as previously described [105]. Briefly, after overnight culture, cells were washed and replenished with Seahorse assay media (Seahorse Bioscience), supplemented with 1 mM pyruvate and 2 mM glutamine. Where applicable, 10 µM BL001 and 1 mM palmitate conjugated to 0.17 mM BSA (150 mM NaCl, pH 7.2), were also added to designated wells. Plates were incubated in a CO_2-free incubator at 37 °C for 1 h to allow temperature and pH equilibration, after which oxygen consumption rate (OCR) was measured in the XF24 Extracellular Flux Analyzer over a period of 95 min. Mitochondrial processes were examined through sequential injections of oligomycin (4 µM) at min 21, carbonyl cyanide

4-(trifluoromethoxy) phenylhydrazone (FCCP; 2 μM) at min 45, 5 μM antimycin A/Rotenone at min 78. At the end of the measurement, cells in each well were counted using the Scepter™ 2.0 Cell Counter to normalize the data. Only the oxygen consumption rate (OCR) for the basal respiration rate was considered for which the area under the curve (AUC) is presented in pertinent figures. Mitochondrial fitness as assessed by the number of non-functional mitochondria in mDCs treated or not with BL001, was determined by flow cytometry using the probes MitoTracker Green that binds covalently to mitochondrial proteins, thus providing an assessment of mass and MitoTracker Red that is taken up by polarized mitochondria thus gauging function. Non-functional mitochondria were then determined by the ratio of MitoTracker Green^{High} over MitoTracker Red^{low} [69]. Fluorescent images were acquired using a Leica TCS SP5 confocal microscope.

RNA extraction and quantitative real-time PCR

Total RNA from was extracted using the RNeasy Micro Kit (Qiagen, Madrid, SP). Complementary DNA using 0.1 to 1 μg RNA was synthesized using the Superscript III Reverse Transcriptase (Invitrogen-Thermo Fisher Scientific, Madrid, Spain). The QRT-PCR was performed on individual cDNAs using SYBR green (Roche) [21]. Gene-specific primers were selected using a human housekeeping gene database (HRT Atlas v1.0 database) [106] and the sequences are listed in the Key Resource Table. Expression levels were normalized to various reference genes including CCNI and ACTIN. The relative gene expression was calculated using the standard curve-based method [107].

Western blot

MDMs were disrupted in a RIPA lysis buffer containing protease (P8340) and phosphatase inhibitors (P0044, P5726). Western blots were performed according to standard methods [105]. Antibodies employed are provided in the Key resources table.

Xenotransplantation

Human islet transplantations were performed as previously described [21]. Briefly, 8-week-old immune-competent C57BL/6J male mice were treated with a single dose of 175 mg /kg b.w. streptozotocin (STZ) prepared in 0.01 M sodium citrate at pH 4.5 to induce hyperglycemia. One week later, mice were anesthetized via an intraperitoneal (*i.p.*) injection of 100 mg/Kg ketamine and 10 mg/Kg xylazine and 750 human islet equivalents (IEQ) were transplanted under the kidney capsule using a PE50 tubing connected to a 25 µL gauged Hamilton syringe. Mice were then *i.p.* injected, or not, with 10 mg/kg body weight (b.w.) BL001. Circulating glucose levels were measured from tail vein blood samples using an Optium Xceed glucometer (Abbott Scientifica SA, Barcelona, Spain). An oral glucose tolerance test (OGTT) was performed at 5-weeks post-transplantation as previously described [108]. Upon termination of the experiment, animals were sacrificed and transplanted kidneys extracted, fixed and embedded for further histological analysis. The entire kidney was sectioned and insulin/glucagon co-immunostaining as well as CD4 was performed at every 15th slice, corresponding with an interval of ~ 75-150 µm which matches the median size of the majority of islets.

Immunofluorescence analyses

For immunostaining, kidneys were fixed overnight in 4% paraformaldehyde at 4ºC. Tissues were dehydrated, paraffin embedded, and sectioned at 5 µm thickness. Immunostaining was then performed overnight at 4°C using a combination of primary antibodies (Key Resources Table) in PBS 1% BSA 0.2% TritonX100. Subsequently, secondary antibodies (Key Resources Table) were incubated for 1 hour at room temperature in PBS 0.2% TritonX100. Nuclei were stained with 0.0001% of 4′,6-diamidino-2-phenylindole (DAPI, Sigma-Aldrich) and cover slips were mounted using fluorescent mounting medium (DAKO). Epifluorescence microscopy images were acquired with a Leica DM6000B microscope and z-stack images were acquired using a Confocal Leica TCS SP5 (AOBS) microscope.

Morphometric analyses

Images of kidney sections were automatically acquired using the Thunder imager software and processed using the Photoshop, ImageJ and FIJI softwares.

QUANTIFICATION AND STATISTICAL ANALYSIS

Data are presented as the mean ± SEM. Student's t-tests were used as described in figure legends. *p* values less than or equal to 0.05 were considered statistically significant. Statistical analyses were performed using the GraphPad Prism software version 8 (GraphPad Software, La Jolla, USA).

REFERENCES

1. Ward, Z.J., Yeh, J.M., Reddy, C.L., Gomber, A., Ross, C., Rittiphairoj, T., Manne-Goehler, J., Abdalla, A.T., Abdullah, M.A., Ahmed, A., et al. (2022). Estimating the total incidence of type 1 diabetes in children and adolescents aged 0-19 years from 1990 to 2050: a global simulation-based analysis. Lancet Diabetes Endocrinol *10*, 848-858. 10.1016/S2213-8587(22)00276-5.
2. Jacobsen, L.M., Newby, B.N., Perry, D.J., Posgai, A.L., Haller, M.J., and Brusko, T.M. (2018). Immune Mechanisms and Pathways Targeted in Type 1 Diabetes. Curr Diab Rep *18*, 90. 10.1007/s11892-018-1066-5.
3. Bonifacio, E., and Achenbach, P. (2019). Birth and coming of age of islet autoantibodies. Clin Exp Immunol *198*, 294–305. 10.1111/cei.13360.
4. DiMeglio, L.A., Evans-Molina, C., and Oram, R.A. (2018). Type 1 diabetes. Lancet *391*, 2449-2462. 10.1016/S0140-6736(18)31320-5.
5. Carvalho, T. (2023). FDA approves first drug to delay type 1 diabetes. Nat Med *29*, 280. 10.1038/d41591-022-00115-y.
6. Atkinson, M.A., Roep, B.O., Posgai, A., Wheeler, D.C.S., and Peakman, M. (2019). The challenge of modulating beta-cell autoimmunity in type 1 diabetes. Lancet Diabetes Endocrinol *7*, 52-64. 10.1016/S2213-8587(18)30112-8.
7. Mallone, R., and Eizirik, D.L. (2020). Presumption of innocence for beta cells: why are they vulnerable autoimmune targets in type 1 diabetes? Diabetologia *63*, 1999-2006. 10.1007/s00125-020-05176-7.
8. Toren, E., Burnette, K.S., Banerjee, R.R., Hunter, C.S., and Tse, H.M. (2021). Partners in Crime: Beta-Cells and Autoimmune Responses Complicit in Type 1 Diabetes Pathogenesis. Front Immunol *12*, 756548. 10.3389/fimmu.2021.756548.
9. Pineros, A.R., Kulkarni, A., Gao, H., Orr, K.S., Glenn, L., Huang, F., Liu, Y., Gannon, M., Syed, F., Wu, W., et al. (2022). Proinflammatory signaling in islet beta cells propagates invasion of pathogenic immune cells in autoimmune diabetes. Cell Rep *39*, 111011. 10.1016/j.celrep.2022.111011.
10. Cobo-Vuilleumier, N., and Gauthier, B.R. (2020). Time for a Paradigm Shift in Treating Type 1 Diabetes Mellitus: Coupling Inflammation to Islet Regeneration. Metabolism *104*, 154137. 10.1016/j.metabol.2020.154137.

11. Frigo, D.E., Bondesson, M., and Williams, C. (2021). Nuclear receptors: from molecular mechanisms to therapeutics. Essays Biochem *65*, 847-856. 10.1042/EBC20210020.
12. Weikum, E.R., Liu, X., and Ortlund, E.A. (2018). The nuclear receptor superfamily: A structural perspective. Protein Sci *27*, 1876-1892. 10.1002/pro.3496.
13. Zhao, L., Zhou, S., and Gustafsson, J.A. (2019). Nuclear Receptors: Recent Drug Discovery for Cancer Therapies. Endocr Rev *40*, 1207-1249. 10.1210/er.2018-00222.
14. Benod, C., Vinogradova, M.V., Jouravel, N., Kim, G.E., Fletterick, R.J., and Sablin, E.P. (2011). Nuclear receptor liver receptor homologue 1 (LRH-1) regulates pancreatic cancer cell growth and proliferation. Proc Natl Acad Sci U S A *108*, 16927-16931. 10.1073/pnas.1112047108.
15. Nadolny, C., and Dong, X. (2015). Liver receptor homolog-1 (LRH-1): a potential therapeutic target for cancer. Cancer Biol Ther *16*, 997-1004. 10.1080/15384047.2015.1045693.
16. Baquie, M., St-Onge, L., Kerr-Conte, J., Cobo-Vuilleumier, N., Lorenzo, P.I., Moreno, C.M., Cederroth, C.R., Nef, S., Borot, S., Bosco, D., et al. (2011). The Liver Receptor Homolog-1 (LRH-1) is Expressed in Human Islets and Protects {beta}-cells Against Stress-Induced Apoptosis. Hum Mol Genet *20*, 2823-2833. 10.1093/hmg/ddr193
17. Zerlotin, R., Arconzo, M., Piccinin, E., and Moschetta, A. (2021). Another One Bites the Gut: Nuclear Receptor LRH-1 in Intestinal Regeneration and Cancer. Cancers (Basel) *13*. 10.3390/cancers13040896.
18. Lee, J.M., Lee, Y.K., Mamrosh, J.L., Busby, S.A., Griffin, P.R., Pathak, M.C., Ortlund, E.A., and Moore, D.D. (2011). A nuclear-receptor-dependent phosphatidylcholine pathway with antidiabetic effects. Nature *474*, 506-510. 10.1038/nature10111.
19. Meng, L., Dong, F., and Deng, J. (2023). NR5A2 as a potential target for exercise to improve metabolic syndrome. Aging (Albany NY) *15*, 2485-2502. 10.18632/aging.204606.
20. Michalek, S., and Brunner, T. (2021). Nuclear-mitochondrial crosstalk: On the role of the nuclear receptor liver receptor homolog-1 (NR5A2) in the regulation of mitochondrial metabolism, cell survival, and cancer. IUBMB Life *73*, 592-610. 10.1002/iub.2386.
21. Cobo-Vuilleumier, N., Lorenzo, P.I., Rodriguez, N.G., Herrera Gomez, I.G., Fuente-Martin, E., Lopez-Noriega, L., Mellado-Gil, J.M., Romero-Zerbo, S.Y., Baquie, M., Lachaud, C.C., et al. (2018). LRH-1 agonism favours an immune-islet dialogue which protects against diabetes mellitus. Nat Commun *9*, 1488. 10.1038/s41467-018-03943-0.
22. Martin Vázquez, E., Cobo-Vuilleumier, N., Araujo Legido, R., Marín-Cañas, S., Nola, E., Dorronsoro, A., López Bermudo, L., Crespo, A., Romero-Zerbo, S.Y., García-Fernández, M., et al. (2022). NR5A2/LRH-1 regulates the PTGS2-PGE2-PTGER1 pathway contributing to pancreatic islet survival and function. iSCIENCE *25*. 10.1016/j.isci.2022.104345.
23. Martín-Vázquez, E., Cobo-Vuilleumier, N., López-Noriega, L., Lorenzo, P.I., and Gauthier, B.R. (2023). The PTGS2/COX2-PGE2 signaling cascade in inflammation: Pro or anti? A case study with type 1 diabetes mellitus. International Journal of Biological Sciences *19*, 4157-4165. 10.7150/ijbs.86492.
24. Ahmed, M., de Winther, M.P.J., and Van den Bossche, J. (2017). Epigenetic mechanisms of macrophage activation in type 2 diabetes. Immunobiology *222*, 937-943. 10.1016/j.imbio.2016.08.011.
25. Di Marco, E., Gray, S.P., and Jandeleit-Dahm, K. (2013). Diabetes alters activation and repression of pro- and anti-inflammatory signaling pathways in the vasculature. Front Endocrinol (Lausanne) *4*, 68. 10.3389/fendo.2013.00068.

26. Danova, K., Grohova, A., Strnadova, P., Funda, D.P., Sumnik, Z., Lebl, J., Cinek, O., Pruhova, S., Kolouskova, S., Obermannova, B., et al. (2017). Tolerogenic Dendritic Cells from Poorly Compensated Type 1 Diabetes Patients Have Decreased Ability To Induce Stable Antigen-Specific T Cell Hyporesponsiveness and Generation of Suppressive Regulatory T Cells. J Immunol *198*, 729-740. 10.4049/jimmunol.1600676.
27. Rodriguez-Fernandez, S., Pujol-Autonell, I., Brianso, F., Perna-Barrull, D., Cano-Sarabia, M., Garcia-Jimeno, S., Villalba, A., Sanchez, A., Aguilera, E., Vazquez, F., et al. (2018). Phosphatidylserine-Liposomes Promote Tolerogenic Features on Dendritic Cells in Human Type 1 Diabetes by Apoptotic Mimicry. Front Immunol *9*, 253. 10.3389/fimmu.2018.00253.
28. Kelly, A., Grabiec, A.M., and Travis, M.A. (2018). Culture of Human Monocyte-Derived Macrophages. Methods Mol Biol *1784*, 1-11. 10.1007/978-1-4939-7837-3_1.
29. Ryu, J.K., Kim, S.J., Rah, S.H., Kang, J.I., Jung, H.E., Lee, D., Lee, H.K., Lee, J.O., Park, B.S., Yoon, T.Y., and Kim, H.M. (2017). Reconstruction of LPS Transfer Cascade Reveals Structural Determinants within LBP, CD14, and TLR4-MD2 for Efficient LPS Recognition and Transfer. Immunity *46*, 38-50. 10.1016/j.immuni.2016.11.007.
30. Veith, A.P., Henderson, K., Spencer, A., Sligar, A.D., and Baker, A.B. (2019). Therapeutic strategies for enhancing angiogenesis in wound healing. Adv Drug Deliv Rev *146*, 97-125. 10.1016/j.addr.2018.09.010.
31. Schlecker, E., Stojanovic, A., Eisen, C., Quack, C., Falk, C.S., Umansky, V., and Cerwenka, A. (2012). Tumor-infiltrating monocytic myeloid-derived suppressor cells mediate CCR5-dependent recruitment of regulatory T cells favoring tumor growth. J Immunol *189*, 5602-5611. 10.4049/jimmunol.1201018.
32. Lu, C.C., Tsai, H.C., Yang, D.Y., Wang, S.W., Tsai, M.H., Hua, C.H., Chen, K.J., Chen, M.Y., Lien, M.Y., and Tang, C.H. (2022). The Chemokine CCL4 Stimulates Angiopoietin-2 Expression and Angiogenesis via the MEK/ERK/STAT3 Pathway in Oral Squamous Cell Carcinoma. Biomedicines *10*. 10.3390/biomedicines10071612.
33. Xuan, W., Qu, Q., Zheng, B., Xiong, S., and Fan, G.H. (2015). The chemotaxis of M1 and M2 macrophages is regulated by different chemokines. J Leukoc Biol *97*, 61-69. 10.1189/jlb.1A0314-170R.
34. Flach, M., and Diefenbach, A. (2015). Chapter 3 - Development of Gut-Associated Lymphoid Tissues. In Mucosal Immunology (Fourth Edition), J. Mestecky, W. Strober, M.W. Russell, B.L. Kelsall, H. Cheroutre, and B.N. Lambrecht, eds. (Academic Press), pp. 31-42. 10.1016/B978-0-12-415847-4.00003-3.
35. Calandra, T., and Roger, T. (2003). Macrophage migration inhibitory factor: a regulator of innate immunity. Nat Rev Immunol *3*, 791-800. 10.1038/nri1200.
36. Maruyama, K., Takada, Y., Ray, N., Kishimoto, Y., Penninger, J.M., Yasuda, H., and Matsuo, K. (2006). Receptor activator of NF-kappa B ligand and osteoprotegerin regulate proinflammatory cytokine production in mice. J Immunol *177*, 3799-3805. 10.4049/jimmunol.177.6.3799.
37. White, G.E., Iqbal, A.J., and Greaves, D.R. (2013). CC chemokine receptors and chronic inflammation--therapeutic opportunities and pharmacological challenges. Pharmacol Rev *65*, 47-89. 10.1124/pr.111.005074.
38. Lindner, M., Thummler, K., Arthur, A., Brunner, S., Elliott, C., McElroy, D., Mohan, H., Williams, A., Edgar, J.M., Schuh, C., et al. (2015). Fibroblast growth factor signalling in multiple sclerosis: inhibition of myelination and induction of pro-inflammatory environment by FGF9. Brain *138*, 1875-1893. 10.1093/brain/awv102.
39. Mattioli, B., Straface, E., Quaranta, M.G., Giordani, L., and Viora, M. (2005). Leptin promotes differentiation and survival of human dendritic cells and licenses them for Th1 priming. J Immunol *174*, 6820-6828. 10.4049/jimmunol.174.11.6820.

40. Felix, F.B., Dias, J., Vago, J.P., Martins, D.G., Beltrami, V.A., Fernandes, D.O., Menezes Dos Santos, A.C.P., Queiroz-Junior, C.M., de Sousa, L.P., Amaral, F.A., et al. (2023). Blocking the HGF-MET pathway induces resolution of neutrophilic inflammation by promoting neutrophil apoptosis and efferocytosis. Pharmacol Res *188*, 106640. 10.1016/j.phrs.2022.106640.
41. Ding, H., and Wu, T. (2018). Insulin-Like Growth Factor Binding Proteins in Autoimmune Diseases. Front Endocrinol (Lausanne) *9*, 499. 10.3389/fendo.2018.00499.
42. Wilson, K.R., Villadangos, J.A., and Mintern, J.D. (2021). Dendritic cell Flt3 - regulation, roles and repercussions for immunotherapy. Immunol Cell Biol *99*, 962-971. 10.1111/imcb.12484.
43. Wang, N., and Tian, B. (2021). Brain-derived neurotrophic factor in autoimmune inflammatory diseases (Review). Exp Ther Med *22*, 1292. 10.3892/etm.2021.10727.
44. van der Kroef, M., Carvalheiro, T., Rossato, M., de Wit, F., Cossu, M., Chouri, E., Wichers, C.G.K., Bekker, C.P.J., Beretta, L., Vazirpanah, N., et al. (2020). CXCL4 triggers monocytes and macrophages to produce PDGF-BB, culminating in fibroblast activation: Implications for systemic sclerosis. J Autoimmun *111*, 102444. 10.1016/j.jaut.2020.102444.
45. Penaranda, C., Kuswanto, W., Hofmann, J., Kenefeck, R., Narendran, P., Walker, L.S., Bluestone, J.A., Abbas, A.K., and Dooms, H. (2012). IL-7 receptor blockade reverses autoimmune diabetes by promoting inhibition of effector/memory T cells. Proc Natl Acad Sci U S A *109*, 12668-12673. 10.1073/pnas.1203692109.
46. Lee, L.F., Logronio, K., Tu, G.H., Zhai, W., Ni, I., Mei, L., Dilley, J., Yu, J., Rajpal, A., Brown, C., et al. (2012). Anti-IL-7 receptor-alpha reverses established type 1 diabetes in nonobese diabetic mice by modulating effector T-cell function. Proc Natl Acad Sci U S A *109*, 12674-12679. 10.1073/pnas.1203795109.
47. Van Sickle, B.J., Simmons, J., Hall, R., Raines, M., Ness, K., and Spagnoli, A. (2009). Increased circulating IL-8 is associated with reduced IGF-1 and related to poor metabolic control in adolescents with type 1 diabetes mellitus. Cytokine *48*, 290-294. 10.1016/j.cyto.2009.08.011.
48. Cano-Cano, F., Gomez-Jaramillo, L., Ramos-Garcia, P., Arroba, A.I., and Aguilar-Diosdado, M. (2022). IL-1beta Implications in Type 1 Diabetes Mellitus Progression: Systematic Review and Meta-Analysis. J Clin Med *11*. 10.3390/jcm11051303.
49. Liu, M., Bai, J., He, S., Villarreal, R., Hu, D., Zhang, C., Yang, X., Liang, H., Slaga, T.J., Yu, Y., et al. (2014). Grb10 promotes lipolysis and thermogenesis by phosphorylation-dependent feedback inhibition of mTORC1. Cell Metab *19*, 967-980. 10.1016/j.cmet.2014.03.018.
50. Ip, W.K.E., Hoshi, N., Shouval, D.S., Snapper, S., and Medzhitov, R. (2017). Anti-inflammatory effect of IL-10 mediated by metabolic reprogramming of macrophages. Science *356*, 513-519. 10.1126/science.aal3535.
51. Yuan, Y., Chen, Y., Peng, T., Li, L., Zhu, W., Liu, F., Liu, S., An, X., Luo, R., Cheng, J., et al. (2019). Mitochondrial ROS-induced lysosomal dysfunction impairs autophagic flux and contributes to M1 macrophage polarization in a diabetic condition. Clin Sci (Lond) *133*, 1759-1777. 10.1042/CS20190672.
52. Bune, A.J., Hayman, A.R., Evans, M.J., and Cox, T.M. (2001). Mice lacking tartrate-resistant acid phosphatase (Acp 5) have disordered macrophage inflammatory responses and reduced clearance of the pathogen, Staphylococcus aureus. Immunology *102*, 103-113. 10.1046/j.1365-2567.2001.01145.x.
53. Rose, A.A., Annis, M.G., Dong, Z., Pepin, F., Hallett, M., Park, M., and Siegel, P.M. (2010). ADAM10 releases a soluble form of the GPNMB/Osteoactivin extracellular domain with angiogenic properties. PLoS One *5*, e12093. 10.1371/journal.pone.0012093.

54. Ledesma-Colunga, M.G., Baschant, U., Weidner, H., Alves, T.C., Mirtschink, P., Hofbauer, L.C., and Rauner, M. (2023). Transferrin receptor 2 deficiency promotes macrophage polarization and inflammatory arthritis. Redox Biol *60*, 102616. 10.1016/j.redox.2023.102616.
55. Matsuda, A., Suzuki, Y., Honda, G., Muramatsu, S., Matsuzaki, O., Nagano, Y., Doi, T., Shimotohno, K., Harada, T., Nishida, E., et al. (2003). Large-scale identification and characterization of human genes that activate NF-kappaB and MAPK signaling pathways. Oncogene *22*, 3307-3318. 10.1038/sj.onc.1206406.
56. Lin, L., Chen, S., Wang, H., Gao, B., Kallakury, B., Bhuvaneshwar, K., Cahn, K., Gusev, Y., Wang, X., Wu, Y., et al. (2021). SPTBN1 inhibits inflammatory responses and hepatocarcinogenesis via the stabilization of SOCS1 and downregulation of p65 in hepatocellular carcinoma. Theranostics *11*, 4232-4250. 10.7150/thno.49819.
57. Zanoni, I., Ostuni, R., Marek, L.R., Barresi, S., Barbalat, R., Barton, G.M., Granucci, F., and Kagan, J.C. (2011). CD14 controls the LPS-induced endocytosis of Toll-like receptor 4. Cell *147*, 868-880. 10.1016/j.cell.2011.09.051.
58. Ciesielska, A., Matyjek, M., and Kwiatkowska, K. (2021). TLR4 and CD14 trafficking and its influence on LPS-induced pro-inflammatory signaling. Cell Mol Life Sci *78*, 1233-1261. 10.1007/s00018-020-03656-y.
59. Cuschieri, J., Gourlay, D., Garcia, I., Jelacic, S., and Maier, R.V. (2004). Implications of proteasome inhibition: an enhanced macrophage phenotype. Cell Immunol *227*, 140-147. 10.1016/j.cellimm.2004.03.005.
60. Choi, S., Dong, B., Lin, C.J., Heo, M.J., Kim, K.H., Sun, Z., Wagner, M., Putluri, N., Suh, J.M., Wang, M.C., and Moore, D.D. (2020). Methyl-Sensing Nuclear Receptor Liver Receptor Homolog-1 Regulates Mitochondrial Function in Mouse Hepatocytes. Hepatology *71*, 1055-1069. 10.1002/hep.30884.
61. Lauterbach, M.A., Hanke, J.E., Serefidou, M., Mangan, M.S.J., Kolbe, C.C., Hess, T., Rothe, M., Kaiser, R., Hoss, F., Gehlen, J., et al. (2019). Toll-like Receptor Signaling Rewires Macrophage Metabolism and Promotes Histone Acetylation via ATP-Citrate Lyase. Immunity *51*, 997-1011 e1017. 10.1016/j.immuni.2019.11.009.
62. Mills, E.L., Kelly, B., Logan, A., Costa, A.S.H., Varma, M., Bryant, C.E., Tourlomousis, P., Dabritz, J.H.M., Gottlieb, E., Latorre, I., et al. (2016). Succinate Dehydrogenase Supports Metabolic Repurposing of Mitochondria to Drive Inflammatory Macrophages. Cell *167*, 457-470 e413. 10.1016/j.cell.2016.08.064.
63. Barcena, C., Mayoral, P., and Quiros, P.M. (2018). Mitohormesis, an Antiaging Paradigm. Int Rev Cell Mol Biol *340*, 35-77. 10.1016/bs.ircmb.2018.05.002.
64. Timblin, G.A., Tharp, K.M., Ford, B., Winchester, J.M., Wang, J., Zhu, S., Khan, R.I., Louie, S.K., Iavarone, A.T., Ten Hoeve, J., et al. (2021). Mitohormesis reprogrammes macrophage metabolism to enforce tolerance. Nat Metab *3*, 618-635. 10.1038/s42255-021-00392-w.
65. Pozzi, L.A., Maciaszek, J.W., and Rock, K.L. (2005). Both dendritic cells and macrophages can stimulate naive CD8 T cells in vivo to proliferate, develop effector function, and differentiate into memory cells. J Immunol *175*, 2071-2081. 10.4049/jimmunol.175.4.2071.
66. Nair, S., Buiting, A.M., Rouse, R.J., Van Rooijen, N., Huang, L., and Rouse, B.T. (1995). Role of macrophages and dendritic cells in primary cytotoxic T lymphocyte responses. Int Immunol *7*, 679-688. 10.1093/intimm/7.4.679.
67. O'Neill, L.A., and Pearce, E.J. (2016). Immunometabolism governs dendritic cell and macrophage function. J Exp Med *213*, 15-23. 10.1084/jem.20151570.
68. Kelly, B., and O'Neill, L.A. (2015). Metabolic reprogramming in macrophages and dendritic cells in innate immunity. Cell Res *25*, 771-784. 10.1038/cr.2015.68.
69. Monteiro, L.B., Davanzo, G.G., de Aguiar, C.F., and Moraes-Vieira, P.M.M. (2020). Using flow cytometry for mitochondrial assays. MethodsX *7*, 100938. 10.1016/j.mex.2020.100938.

70. Mnasria, K., Lagaraine, C., Velge-Roussel, F., Oueslati, R., Lebranchu, Y., and Baron, C. (2008). Anti-CD25 antibodies affect cytokine synthesis pattern of human dendritic cells and decrease their ability to prime allogeneic CD4+ T cells. J Leukoc Biol *84*, 460-467. 10.1189/jlb.1007712.
71. Atkinson, M.A., and Mirmira, R.G. (2023). The pathogenic "symphony" in type 1 diabetes: A disorder of the immune system, beta cells, and exocrine pancreas. Cell Metab. 10.1016/j.cmet.2023.06.018.
72. Penna, G., and Adorini, L. (2000). 1 Alpha,25-dihydroxyvitamin D3 inhibits differentiation, maturation, activation, and survival of dendritic cells leading to impaired alloreactive T cell activation. J Immunol *164*, 2405-2411. 10.4049/jimmunol.164.5.2405.
73. van Halteren, A.G., van Etten, E., de Jong, E.C., Bouillon, R., Roep, B.O., and Mathieu, C. (2002). Redirection of human autoreactive T-cells Upon interaction with dendritic cells modulated by TX527, an analog of 1,25 dihydroxyvitamin D(3). Diabetes *51*, 2119-2125. 10.2337/diabetes.51.7.2119.
74. Wagner, L.E., Melnyk, O., Duffett, B.E., and Linnemann, A.K. (2022). Mouse models and human islet transplantation sites for intravital imaging. Front Endocrinol (Lausanne) *13*, 992540. 10.3389/fendo.2022.992540.
75. Atkinson, M.A., Eisenbarth, G.S., and Michels, A.W. (2014). Type 1 diabetes. Lancet *383*, 69-82. 10.1016/S0140-6736(13)60591-7.
76. Van den Bossche, J., Baardman, J., Otto, N.A., van der Velden, S., Neele, A.E., van den Berg, S.M., Luque-Martin, R., Chen, H.J., Boshuizen, M.C., Ahmed, M., et al. (2016). Mitochondrial Dysfunction Prevents Repolarization of Inflammatory Macrophages. Cell Rep *17*, 684-696. 10.1016/j.celrep.2016.09.008.
77. Patsalos, A., Halasz, L., Medina-Serpas, M.A., Berger, W.K., Daniel, B., Tzerpos, P., Kiss, M., Nagy, G., Fischer, C., Simandi, Z., et al. (2022). A growth factor-expressing macrophage subpopulation orchestrates regenerative inflammation via GDF-15. J Exp Med *219*. 10.1084/jem.20210420.
78. Nakayasu, E.S., Syed, F., Tersey, S.A., Gritsenko, M.A., Mitchell, H.D., Chan, C.Y., Dirice, E., Turatsinze, J.V., Cui, Y., Kulkarni, R.N., et al. (2020). Comprehensive Proteomics Analysis of Stressed Human Islets Identifies GDF15 as a Target for Type 1 Diabetes Intervention. Cell Metab *31*, 363-374 e366. 10.1016/j.cmet.2019.12.005.
79. Tello-Montoliu, A., Patel, J.V., and Lip, G.Y. (2006). Angiogenin: a review of the pathophysiology and potential clinical applications. J Thromb Haemost *4*, 1864-1874. 10.1111/j.1538-7836.2006.01995.x.
80. Yamasaki, S., Ivanov, P., Hu, G.F., and Anderson, P. (2009). Angiogenin cleaves tRNA and promotes stress-induced translational repression. J Cell Biol *185*, 35-42. 10.1083/jcb.200811106.
81. Czech, A., Wende, S., Morl, M., Pan, T., and Ignatova, Z. (2013). Reversible and rapid transfer-RNA deactivation as a mechanism of translational repression in stress. PLoS Genet *9*, e1003767. 10.1371/journal.pgen.1003767.
82. Pujol-Autonell, I., Ampudia, R.M., Planas, R., Marin-Gallen, S., Carrascal, J., Sanchez, A., Marin, A., Puig-Domingo, M., Pujol-Borrell, R., Verdaguer, J., and Vives-Pi, M. (2013). Efferocytosis promotes suppressive effects on dendritic cells through prostaglandin E2 production in the context of autoimmunity. PLoS One *8*, e63296. 10.1371/journal.pone.0063296.
83. Herold, K.C., Bucktrout, S.L., Wang, X., Bode, B.W., Gitelman, S.E., Gottlieb, P.A., Hughes, J., Joh, T., McGill, J.B., Pettus, J.H., et al. (2019). Immunomodulatory activity of humanized anti-IL-7R monoclonal antibody RN168 in subjects with type 1 diabetes. JCI Insight *4*, e126054. 10.1172/jci.insight.126054.
84. Harris, J., Deen, N., Zamani, S., and Hasnat, M.A. (2018). Mitophagy and the release of inflammatory cytokines. Mitochondrion *41*, 2-8. 10.1016/j.mito.2017.10.009.

85. Brusko, T.M., Wasserfall, C.H., Clare-Salzler, M.J., Schatz, D.A., and Atkinson, M.A. (2005). Functional defects and the influence of age on the frequency of CD4+ CD25+ T-cells in type 1 diabetes. Diabetes *54*, 1407-1414. 10.2337/diabetes.54.5.1407.
86. Lindley, S., Dayan, C.M., Bishop, A., Roep, B.O., Peakman, M., and Tree, T.I. (2005). Defective suppressor function in CD4(+)CD25(+) T-cells from patients with type 1 diabetes. Diabetes *54*, 92-99. 10.2337/diabetes.54.1.92.
87. Bluestone, J.A., Buckner, J.H., Fitch, M., Gitelman, S.E., Gupta, S., Hellerstein, M.K., Herold, K.C., Lares, A., Lee, M.R., Li, K., et al. (2015). Type 1 diabetes immunotherapy using polyclonal regulatory T cells. Sci Transl Med *7*, 315ra189. 10.1126/scitranslmed.aad4134.
88. Marek-Trzonkowska, N., Mysliwiec, M., Dobyszuk, A., Grabowska, M., Derkowska, I., Juscinska, J., Owczuk, R., Szadkowska, A., Witkowski, P., Mlynarski, W., et al. (2014). Therapy of type 1 diabetes with CD4(+)CD25(high)CD127-regulatory T cells prolongs survival of pancreatic islets - results of one year follow-up. Clin Immunol *153*, 23-30. 10.1016/j.clim.2014.03.016.
89. Dong, S., Hiam-Galvez, K.J., Mowery, C.T., Herold, K.C., Gitelman, S.E., Esensten, J.H., Liu, W., Lares, A.P., Leinbach, A.S., Lee, M., et al. (2021). The effect of low-dose IL-2 and Treg adoptive cell therapy in patients with type 1 diabetes. JCI Insight *6*. 10.1172/jci.insight.147474.
90. Ramzy, A., Thompson, D.M., Ward-Hartstonge, K.A., Ivison, S., Cook, L., Garcia, R.V., Loyal, J., Kim, P.T.W., Warnock, G.L., Levings, M.K., and Kieffer, T.J. (2021). Implanted pluripotent stem-cell-derived pancreatic endoderm cells secrete glucose-responsive C-peptide in patients with type 1 diabetes. Cell Stem Cell *28*, 2047-2061 e2045. 10.1016/j.stem.2021.10.003.
91. Shapiro, A.M.J., Thompson, D., Donner, T.W., Bellin, M.D., Hsueh, W., Pettus, J., Wilensky, J., Daniels, M., Wang, R.M., Brandon, E.P., et al. (2021). Insulin expression and C-peptide in type 1 diabetes subjects implanted with stem cell-derived pancreatic endoderm cells in an encapsulation device. Cell Rep Med *2*, 100466. 10.1016/j.xcrm.2021.100466.
92. Lablanche, S., Vantyghem, M.C., Kessler, L., Wojtusciszyn, A., Borot, S., Thivolet, C., Girerd, S., Bosco, D., Bosson, J.L., Colin, C., et al. (2018). Islet transplantation versus insulin therapy in patients with type 1 diabetes with severe hypoglycaemia or poorly controlled glycaemia after kidney transplantation (TRIMECO): a multicentre, randomised controlled trial. Lancet Diabetes Endocrinol *6*, 527-537. 10.1016/S2213-8587(18)30078-0.
93. Parent, A.V., Faleo, G., Chavez, J., Saxton, M., Berrios, D.I., Kerper, N.R., Tang, Q., and Hebrok, M. (2021). Selective deletion of human leukocyte antigens protects stem cell-derived islets from immune rejection. Cell Rep *36*, 109538. 10.1016/j.celrep.2021.109538.
94. Gerace, D., Zhou, Q., Kenty, J.H., Veres, A., Sintov, E., Wang, X., Boulanger, K.R., Li, H., and Melton, D.A. (2023). Engineering human stem cell-derived islets to evade immune rejection and promote localized immune tolerance. Cell Rep Med *4*, 100879. 10.1016/j.xcrm.2022.100879.
95. Leite, N.C., Sintov, E., Meissner, T.B., Brehm, M.A., Greiner, D.L., Harlan, D.M., and Melton, D.A. (2020). Modeling Type 1 Diabetes In Vitro Using Human Pluripotent Stem Cells. Cell Rep *32*, 107894. 10.1016/j.celrep.2020.107894.
96. Perez-Riverol, Y., Bai, J., Bandla, C., Garcia-Seisdedos, D., Hewapathirana, S., Kamatchinathan, S., Kundu, D.J., Prakash, A., Frericks-Zipper, A., Eisenacher, M., et al. (2022). The PRIDE database resources in 2022: a hub for mass spectrometry-based proteomics evidences. Nucleic Acids Res *50*, D543-D552. 10.1093/nar/gkab1038.
97. Kilkenny, C., Browne, W., Cuthill, I.C., Emerson, M., Altman, D.G., and Group, N.C.R.R.G.W. (2010). Animal research: reporting in vivo experiments: the ARRIVE guidelines. Br J Pharmacol *160*, 1577-1579. 10.1111/j.1476-5381.2010.00872.x.

98. Rappsilber, J., Mann, M., and Ishihama, Y. (2007). Protocol for micro-purification, enrichment, pre-fractionation and storage of peptides for proteomics using StageTips. Nat Protoc *2*, 1896-1906. 10.1038/nprot.2007.261.
99. Tyanova, S., Temu, T., and Cox, J. (2016). The MaxQuant computational platform for mass spectrometry-based shotgun proteomics. Nat Protoc *11*, 2301-2319. 10.1038/nprot.2016.136.
100. Tyanova, S., Temu, T., Sinitcyn, P., Carlson, A., Hein, M.Y., Geiger, T., Mann, M., and Cox, J. (2016). The Perseus computational platform for comprehensive analysis of (prote)omics data. Nat Methods *13*, 731-740. 10.1038/nmeth.3901.
101. Goedhart, J., and Luijsterburg, M.S. (2020). VolcaNoseR is a web app for creating, exploring, labeling and sharing volcano plots. Sci Rep *10*, 20560. 10.1038/s41598-020-76603-3.
102. Szklarczyk, D., Gable, A.L., Lyon, D., Junge, A., Wyder, S., Huerta-Cepas, J., Simonovic, M., Doncheva, N.T., Morris, J.H., Bork, P., et al. (2019). STRING v11: protein-protein association networks with increased coverage, supporting functional discovery in genome-wide experimental datasets. Nucleic Acids Res *47*, D607-D613. 10.1093/nar/gky1131.
103. Shannon, P., Markiel, A., Ozier, O., Baliga, N.S., Wang, J.T., Ramage, D., Amin, N., Schwikowski, B., and Ideker, T. (2003). Cytoscape: a software environment for integrated models of biomolecular interaction networks. Genome Res *13*, 2498-2504. 10.1101/gr.1239303.
104. Nandakumar, M.P., Shen, J., Raman, B., and Marten, M.R. (2003). Solubilization of trichloroacetic acid (TCA) precipitated microbial proteins via naOH for two-dimensional electrophoresis. J Proteome Res *2*, 89-93. 10.1021/pr025541x.
105. Lopez-Noriega, L., Capilla-Gonzalez, V., Cobo-Vuilleumier, N., Martin-Vazquez, E., Lorenzo, P.I., Martinez-Force, E., Soriano-Navarro, M., Garcia-Fernandez, M., Romero-Zerbo, S.Y., Bermudez-Silva, F.J., et al. (2019). Inadequate control of thyroid hormones sensitizes to hepatocarcinogenesis and unhealthy aging. Aging (Albany NY) *11*, 7746-7779. 10.18632/aging.102285.
106. Hounkpe, B.W., Chenou, F., de Lima, F., and De Paula, E.V. (2021). HRT Atlas v1.0 database: redefining human and mouse housekeeping genes and candidate reference transcripts by mining massive RNA-seq datasets. Nucleic Acids Res *49*, D947-D955. 10.1093/nar/gkaa609.
107. Mellado-Gil, J.M., Fuente-Martin, E., Lorenzo, P.I., Cobo-Vuilleumier, N., Lopez-Noriega, L., Martin-Montalvo, A., Gomez, I.G.H., Ceballos-Chavez, M., Gomez-Jaramillo, L., Campos-Caro, A., et al. (2018). The type 2 diabetes-associated HMG20A gene is mandatory for islet beta cell functional maturity. Cell Death Dis *9*, 279. 10.1038/s41419-018-0272-z.
108. Romero-Zerbo, S.Y., Ruz-Maldonado, I., Espinosa-Jimenez, V., Rafacho, A., Gomez-Conde, A.I., Sanchez-Salido, L., Cobo-Vuilleumier, N., Gauthier, B.R., Tinahones, F.J., Persaud, S.J., and Bermudez-Silva, F.J. (2017). The cannabinoid ligand LH-21 reduces anxiety and improves glucose handling in diet-induced obese pre-diabetic mice. Sci Rep *7*, 3946. 10.1038/s41598-017-03292-w.

FIGURE LEGENDS

FIGURE 1: LRH-1/NR5A2 activation reduces pro-inflammatory cell surface markers in monocyte-derived macrophages (MDM) and mature dendritic cells (mDCs) from individuals with T1DM. Flow cytometry was used to analyze the following MDM cell surface markers:
(**A**) CD80,
(**B**) CD14,
(**C**) CD206,
(**D**) CD209;
and the following DC cell surface markers:
(**E**) CD36,
(**F**) CD54,
(**G**) CXCR4,
(**H**) CD25.
Measurements were normalized to the mean fluorescence intensity (MFI) of untreated MDM1 or mDC for comparison. A total of *n=5* independent healthy individuals and *n=10* independent individuals with T1DM were analyzed for MDM, while *n=9* independent healthy individuals and *n=9* independent individuals with T1DM were evaluated for mDCs markers. Each donor is colour-coded. Data are presented as means ± SEM and compared to either untreated MDM1 or mDC from either healthy or T1DM individuals. Paired Student t-test * $p<0.05$, ** $p<0.01$ and *** $p<0.001$ as compared to untreated cells ($MDM1_0$, MDM1, iDC and mDC). Flow cytometry histograms (untreated: orange, and BL001 treated: blue) as well as estimation plots (linked to plots by either & or #) are shown only for the markers with statistically significant differences.

FIGURE 2: Pharmacological activation of LRH-1/NR5A2 changes the cytokine secretion profile of monocyte-derived macrophages (MDM) and dendritic cells (DCs) isolated from individuals with T1DM. The cytokine secretion profile was assessed for:
(**A**) $MDM1_0$,
(**B**) MDM1,
(**C**) iDCs,
(**D**) mDCs
A total of *n=3* independent donors were analyzed for $MDM1_0$, while *n=5* independent individuals were evaluated for MDM1, iDCs, mDCs. Percent changes in cytokine secretion are presented relative to DMSO-treated counterparts for each cytokine. Only significantly altered cytokines are shown. Data are presented as percent changes compared to DMSO for each cytokine. Unpaired Student t-test * $p<0.05$, ** $p<0.01$, *** $p<0.001$, **** $p<0.001$ compared to DMSO

FIGURE 3: LRH-1/NR5A2 agonism mitigates the pro-inflammatory program in T1DM monocyte-derived macrophages (MDM).
(**A**) Heatmap illustrating the most differentially expressed genes between untreated healthy (*n=3* independent donors) and untreated T1DM (*n=4* independent donors) individuals in non-activated ($MDM1_0$) or activated (MDM1) macrophages. Gene expression levels are presented as log-transformed normalized counts (log(NC)).
(**B**) Volcano plot of differentially expressed genes in BL001-treated vs untreated $MDM1_0$ (*n=6* independent donors).
(**C**) Dot plot of KEGG pathways enriched in BL001-treated $MDM1_0$.
(**D**) Cnetplots of selected KEGG pathways modulated by BL001 in $MDM1_0$. Arrows point to genes of interest which are described in the results section.
(**E**) Volcano plot of differentially expressed genes in BL001-treated vs untreated MDM1 (*n=6*, independent donors)
(**F**) Dot plot of KEGG pathways enriched in BL001-treated MDM1.

(**G**) Cnetplots of selected KEGG pathways modulated by BL001 in MDM1. Arrows highlight genes of interest which are described in the results.

FIGURE 4: Proteomic alterations induced by BL001 in T1DM monocyte-derived macrophages (MDM).
(**A**) Volcano plot displaying the most significantly differentially expressed proteins in BL001-treated versus untreated $MDM1_0$, derived from *n=3* independent donors. Arrows point to genes of interest which are described in the results section.
(**B**) Volcano plot displaying the most significantly differentially expressed proteins in BL001-treated versus untreated MDM1, from *n=3* independent donors. Arrows point to genes of interest which are described in the results section.
(**C**) Cytoscape circular layout of significantly up-regulated proteins in BL001-treated $MDM1_0$ compared to untreated controls. RNA-associated proteins are highlighted within the grey-shaded area. Arrows point to genes of interest which are described in the results section.
(**D**) Cytoscape circular layout of significantly down-regulated proteins in BL001-treated $MDM1_0$. as compared to untreated $MDM1_0$, with mitochondrial proteins emphasized by the pink-shaded area.
(**E**) InteractiVenn diagram of differentially expressed genes that are significantly altered in either the RNAseq or proteomic analysis of BL001-treated versus untreated $MDM1_0$.
(**F**) Heatmap of differentially expressed genes common to both the RNAseq and proteomic analysis in BL001-treated $MDM1_0$ versus untreated $MDM1_0$ marked by green circles in (E). Arrows point to genes of interest which are described in the results section.
(**G**) Cytoscape circular layout of significantly up-regulated proteins in BL001-treated MDM1 as compared to untreated MDM1. Proteins involved in transcriptional/translational processes are within the French beige-shaded area.
(**H**) Cytoscape circular layout of significantly down-regulated proteins in BL001-treated MDM1 as compared to untreated MDM1. Mitochondrial proteins are highlighted in the pink shaded area, while proteasome-associated proteins are in the blue-shaded area.
(**I**) InteractiVenn diagram of differentially expressed genes that are significantly altered in either the RNAseq or proteomic analysis of BL001-treated versus untreated MDM1. Arrow point to a gene of interest which is described in the results section.
(**J**) Heatmap of differentially expressed genes common to both RNAseq and proteomic analysis of BL001-treated $MDM1_0$ versus untreated $MDM1_0$ (red circles in I). Red arrow; CD14
(**K**) Bar graph representing acetyl CoA levels in MDM1 treated or not with BL001 for *n=3* independent donors colour-coded and each performed in triplicate. Data are presented as means ± SEM. Student t-test * $p<0.05$ as compared to untreated. Arrows point to genes of interest which are described in the results section.

FIGURE 5: LRH-1/NR5A2 activation stimulates mitohormesis to enforce LPS-tolerance in T1DM MDM1.
(**A**) Mitochondrial stress test performed on T1DM $MDM1_0$ and MDM1 (namely LPS/IFNγ-treated $MDM1_0$) treated with or without BL001. *n=4* independent donors.
(**B**) Calculated basal oxygen consumption rates (OCR-BR) Abbreviations: Oligo-Oligomycin, FCCP-Carbonyl cyanide-p-trifluoromethoxyphenylhydrazone, Rot-Rotenone, Ant-Antimycin A. Paired Student t-test **$p<0.01$ as compared to $MDM1_0$ or MDM1. *n=4* independent colour-coded donors.
(**C**) Transcript levels of the mitohormesis-associated gene ATF4, in BL001 treated or not MDM1 cells from T1DM donors, normalized to the housekeeping gene CCNI (https://housekeeping.unicamp.br/). *n=5* independent colour-coded donors.
(**D**) Protein expression levels of ATF4 in BL001 treated or not MDM1 cells from T1DM individuals, and normalized to the housekeeping protein β-actin. *n=3* independent colour-coded donors. The figure includes a representative western blot image.

(**E-G**) Transcript levels of GDF15, IL-1β, and NLRP3 in T1DM MDM1 treated with or without BL001. Transcript levels were normalized to the housekeeping gene CCNI (https://housekeeping.unicamp.br/). *n=5* independent colour-coded donors. Data are presented as means ± SEM. Paired Student t-test * p<0.05, **p<0.01 as compared to untreated cells.
(**H and I**) Relative proliferation of autologous $CD4^+$ and $CD8^+$ T cells in response to co-culture with healthy or T1DM MDMs treated or not with 10 μM BL001. *n=4* independent colour-coded donors. Paired Student t-test *p<0.05 as compared to untreated cells.

FIGURE 6: Pharmacological activation of LRH-1/NR5A2 fosters a tolerogenic gene signature profile in mDCs isolated from individuals with T1DM.
(**A**) Heatmap of the most differentially expressed genes between healthy individuals (*n=5* independent donors) and those with T1DM (*n=4* independent donors) in immature DCs (iDC) or mature DCs (mDC). Gene expression is presented as log-transformed normalized counts (log(NC)).
(**B**) Volcano plot of differentially expressed genes in BL001-treated vs untreated iDCS (*n=5* independent donors)
(**C**) Volcano plots of differentially expressed genes in BL001-treated vs untreated mDCs (*n=4* independent donors)
(**D**) Dot plot of KEGG pathways enriched in BL001-treated mDCs. Arrows point to pathways of interest which are described in the results section.
(**E**) Cnetplots of selected KEGG pathways modulated by BL001 in mDCs.
(**F**) Heatmap of selected genes associated with a tolerogenic DC phenotype. Gene expression is presented as the average log(NC) of n=4 independent donors.

FIGURE 7: Pharmacological activation of LRH-1/NR5A2 induces mitochondria turnover to inactivate T1DM mDCs, thereby reducing autologous $CD4^+$ and $CD8^+$ T-cell proliferation stimulation.
(**A-B**) Mitochondrial stress test and calculated basal oxygen consumption rates (OCR) in T1DM iDC and mDC treated with or without BL001 and with palmitate. Abbreviations: Oligo-Oligomycin, FCCP-Carbonyl cyanide-p-trifluoromethoxyphenylhydrazone, Rot-Rotenone, Ant-Antimycin A. *n=4* independent donors (colour matched). Paired Student t-test ** p<0.01 as compared to iDCs. Each donor is colour-coded.
(**C**) Representative confocal immunofluorescence images of cells labeled with MitoTracker green and MitoTracker red for mitochondria, with nuclei counterstained using DAPI. Alongside, a bar chart quantification for mitochondrial functionality, as determined by flow cytometry based on these two markers. Representative flow cytometry plots are provided for illustration. *n=3* independent colour-code donors. Paired Student t-test ** p<0.01 as compared to untreated mDC.
(**D-E**) Relative autologous proliferation of $CD4^+$ and $CD8^+$ T-cells in the presence of either healthy or T1DM DCs treated with or without 10 μM BL001. Data are presented as means ± SEM. Paired Student t-test * p<0.05 as compared to untreated cells.

FIGURE 8: LRH-1/NR5A2 agonism promotes the expansion of a $CD4^+/CD25^+/FoxP3^+$ cell subpopulation, leading to reduced $CD8^+$ T-cell proliferation in T1DM individuals.
(A) Representative flow cytometry plots depicting the percentage of $CD25^+$ and $FoxP3^+$ cells within the $CD4^+$ subpopulation and quantification thereof (*n=8* independent healthy and T1DM donors, colour-matched). Flow cytometry histograms (untreated: orange, and BL001 treated: blue) as well as estimation plots are shown only for statistically significant differences. Results are presented as the percentage of the $CD4^+$ subpopulation. *p<0.05 paired Student t-test.
(**B-C**) $CD14^-$ PBMCs were labelled with CFSE and stimulated/expanded using a polymeric nanomatrix structure composed of CD3 and CD28 for 24 hours before the addition of $CD4^+$ T-cells (at a 1:2 ratio, respectively). Proliferation of (**B**) $CD4^+/CFSE^+$

and (**C**) $CD8^+/CFSE^+$ subpopulations was assessed by flow cytometry 4 days post co-culturing. Data are presented as means ± SEM. n=4 healthy and n=6 T1DM independent donors. **p<0.01 Paired Student t-test.

FIGURE 9: BL001 improves human islet graft survival and function in STZ-treated immunocompetent C57BL/6j mice. (**A**) Experimental design of the 4-week BL001 treatment post-xenotransplantation experiment. Eight-week-old C57BL/6j were treated with streptozotocin (STZ;175 mg/Kg body weight) to induce hyperglycemia. Seven days later, upon reaching hyperglycemia (non-fasting blood glucose levels >300 mg/dl on two consecutive tests), 750 IEQ human islets from 2 independent donors (characteristics of donors are provided in the table) were transplanted under the kidney capsule of a total of 20 mice. Starting 7 days post-transplant, mice received either vehicle (*n=10*) or BL001,(*n=10*) for 4 weeks. Additionally, seven untreated mice were used as controls for the oral glucose tolerance test (OGTT) and mouse c-peptide level measurements.
(**B**) Weekly measurement of non-fasting blood glucose
(**C**) Kaplan-Meier survival curve.
(**D**) OGTT performed at 4 weeks post-BL001/Vehicle treatment. Mice were fasted for 6 hours before the OGTT.
(**E**) Area under the curve (AUC) corresponding to the OGTT. Student t-test, # *p=0003* and & *p=0.0037* as compared to control non-STZ mice.
(**F**) Human C-peptide plasma levels at 4 weeks post-BL001/Vehicle treatment. Data are presented as means ± SEM. *p<0.05 student t-test.
(**G**) Mouse C-peptide plasma levels at 4 weeks post-BL001/Vehicle treatment. Data are presented as means ± SEM. Student t-test, # *p=002* and & *p=0.0003* as compared to control non-STZ mice.
(**H**) Representative immunofluorescence images of kidney sections from mice euthanized at 4 weeks post-BL001/Vehicle treatment, displaying staining for insulin (INS), glucagon (GCG) staining along with nuclear DAPI staining.
(**I, J, K**) Quantitative analysis of insulin (INS), glucagon (GCG), and $CD4^+$ areas, normalized to the DAPI-positive area per graft, at 4 weeks post BL001 treatment.
(**L**) Experimental design of the 8-week BL001 treatment post-xenotransplantation experiment. Eight-week-old C57BL/6j were treated with streptozotocin (STZ;175 mg/Kg body weight) to induce hyperglycemia. Seven days later, upon reaching hyperglycemia (non-fasting blood glucose levels >300 mg/dl on two consecutive tests), 750 IEQ human islets from 1 donor (characteristics of the donor are provided in the table) were transplanted under the kidney capsule of a total of 14 mice. Starting 7 days post-transplant, mice received either vehicle (*n=7*) or BL001(*n=7*) for 8 weeks. Additionally, six untreated mice were used as controls for c-peptide level measurements.
(**M**) Weekly measurement of non-fasting glycemia.
(**N**) Kaplan Meier survival curve.
(**O**) Human C-peptide plasma levels at 6-week vehicle-treated mice and 8-week BL001-treated mice. Data are presented as means ± SEM. **p<0.01 student t-test.
(**P**) Mouse C-peptide plasma levels at 6-week vehicle-treated mice and 8-week BL001-treated mice. Data are presented as means ± SEM. # *p=0001* and & *p=0.*0002 Student t-test as compared to control non-STZ mice.
(**Q**) Representative immunofluorescence images of kidney sections from mice at 6 weeks post-vehicle treatment and at 8 weeks post-BL001 treatment, displaying staining for insulin (INS), glucagon (GCG) staining along with nuclear DAPI staining.
(**R,S,T**) Quantitative analysis of insulin (INS), glucagon (GCG), and $CD4^+$ areas normalized to the DAPI-positive area per graft, at either 6 weeks post vehicle or 8 weeks post BL001 treatment. Data are presented as means ± SEM. *p<0.05 and ****p<0.0001 student t-test. ns, non-significant.

FIGURE 10: Cellular and molecular mechanism of action mediated by the pharmacological effect of LRH-1/NR5A2 in human cells. Proposed model of genetic

and immune cell-tailored reprogramming induced by LRH-1/NR5A2 activation and its impact on T-effector cell proliferation. Improvement of human islet engraftment influenced by LRH-1/NR5A2 activation.

Key Resources Table

REAGENT or RESOURCE	SOURCE	IDENTIFIER
Antibodies		
CCR7 PECy7	BD Biosciences	Cat#557648
Annexin V PE	Immunotools	Cat#31490014 7
CD3 PE	Immunotools	Cat#21620034
CD4 APC	Immunotools	Cat#21278046
CD8 FITC	Immunotools	Cat#21810083
CD11c APC	Immunotools	Cat#21487116
CD14 PE	Immunotools	Cat#21620144
CD25 PE	Immunotools	Cat#21810254
CD40 APC	Immunotools	Cat#21270406
CD86 FITC	Immunotools	Cat#21480863
HLA class I FITC	Immunotools	Cat#21159033
HLA class II FITC	Immunotools	Cat#21388993
αvβ5 integrin PE	BioLegend	Cat#920007
CD36 APCCy7	BioLegend	Cat#336213
CD54 PECy7	BioLegend	Cat#353115
CCR2 APC	BioLegend	Cat#357207
CXCR4 APCCy7	BioLegend	Cat#306528
TIM4 APC	BioLegend	Cat#354008
DC-SIGN APC	BioLegend	Cat#330108
PD-L1 PECy7	BioLegend	Cat#329717
CTV Cell Proliferation Kit	ThermoFisher Scientific	Cat#C34557
CSFE	ThermoFisher Scientific	Cat#C34554
Zombie Violet 421	BioLegend	Cat#423114
CD4	Miltenyi Biotec	Cat#130-122-994
CD8	eBioscience	Cat#45-0088-41
CD14	BioLegend	Cat#325604
CD25	Miltenyi Biotec	Cat#130-122-994
CD80	Miltenyi Biotec	Cat#130-123-253
CD86	BioLegend	Cat#305412
CD163	Miltenyi Biotec	Cat#130-112-126
CD206	Miltenyi Biotec	Cat#130-095-131
CD200R	Miltenyi Biotec	Cat#130-111-290
CD209	Miltenyi Biotec	Cat#130-092-873
FoxP3	Miltenyi Biotec	Cat#130-122-994
ACTIN	Sigma-Aldrich	Cat#A5441
ATF4	Cell Signaling	Cat#11815
INSULIN	Sigma-Aldrich	Cat#I2018
GLUCAGON	Cell Signaling	Cat#2760
Biological samples		
Human islets	ADI IsletCore Laboratory, Edmonton, CA and Vita-Salute San Raffaele University, Milan (IT)	N/A

Blood samples	Hospital Germans trias I Pujol, Badalona and the University Hospital Virgen Macarena, Sevilla (ES)	N/A
Chemicals, peptides, and recombinant proteins		
BL001	In house	In house
rhIL-4	Prospec	Cat#CYT-211
rhGM-CSF	Prospec	Cat#CYT-221
Human insulin	Sigma-Aldrich	Cat#I3536
TNFα	Immunotools	Cat#11343015
IL-1β	Immunotools	Cat#11340013
PGE2	Cayman Chemical	Cat#14010
Streptozotocin	Sigma-Aldrich/Merck	Cat#S0130-1G
Penicillin	Sigma-Aldrich/Merck	Cat#P0781
Streptomycin	Sigma-Aldrich/Merck	Cat#P0781
INFγ	Immunotools	Cat#11343536
LPS	Sigma-Aldrich/Merck	Cat# L6529
Critical commercial assays		
Cell Mito Stress Test Kit	Agilent	Cat#103015-100
Treg Phenotyping Kit, anti-human, REAfinity	Miltenyi Biotec	Cat#130-122-994
Human Cytokine Array C5	RayBiotech	Cat#AAH-CYT-5-2
Human C-peptide ELISA kit	Mercodia	Cat#10-1136-01
Acetyl Coenzyme A assay kit	Sigma-Aldrich	Car#MAK039-1KT
CD4+ T cell isolation kit	Stemcell Technology	Cat# 17952
Deposited data		
RNAseq dataset	This paper	PRJNA1017470
Proteomic dataset	This paper	PXD045222
Experimental models: Organisms/strains		
C57BL/6J	Janvier Labs	strain code 027/SC-C57J-F
Oligonucleotides		
Primer: ATF4 Fw: TCAAACCTCATGGGTTCTCC Rv: GTGTCATCCAACGTGGTCAG		
Primer: CCNI Fw: GCACAGATGGATAGCTCC Rv: CTTTGTCACAGGTCACCA		
Primer: GDF15 Fw: ACCTGCACCTGCGTATCTCT Rv:CGGACGAAGATTCTGCCAG		
Primer: IL1B Fw: AGCTACGAATCTCCGACCAC Rv: CGTTATCCCATGTGTCGAAGAA		
Primer: NLRP3 Fw: CGTGAGTCCCATTAAGATGGAGT Rv: CCCGACAGTGGATATAGAACAGA		
Software and algorithms		
FlowJo software	Tree Star Inc	www.flowjo.com
Fiji	Imagej	https://imagej.net/software/fiji/downloads
Prism	GraphPad	https://www.graphpad.com/
Adobe Photoshop	Adobe	https://www.adobe.com/es/
ImageJ	Imagej	https://imagej.nih.gov/ij/

Cytoscape	Cytoscape	https://cytoscape.org/index.html
Other		
BD Vacutainer Sodium Heparin tubes	BD	Cat#366667
Ficoll Paque PLUS	Cytiva	Cat#17144003
Histopaque 1077	Sigma-Aldrich	Cat#10771
EasySep Human CD14 Positive Selection kit II	STEMCELL Technologies	Cat#17858
Accutase	ThermoFisher Scientific	Cat#00-4555-56
7-AAD	BD Biosciences	Cat#559925
MitoTracker Green	ThermoFisher Scientific	Cat#M7514
MitoTracker Red	ThermoFisher Scientific	Cat#M7512

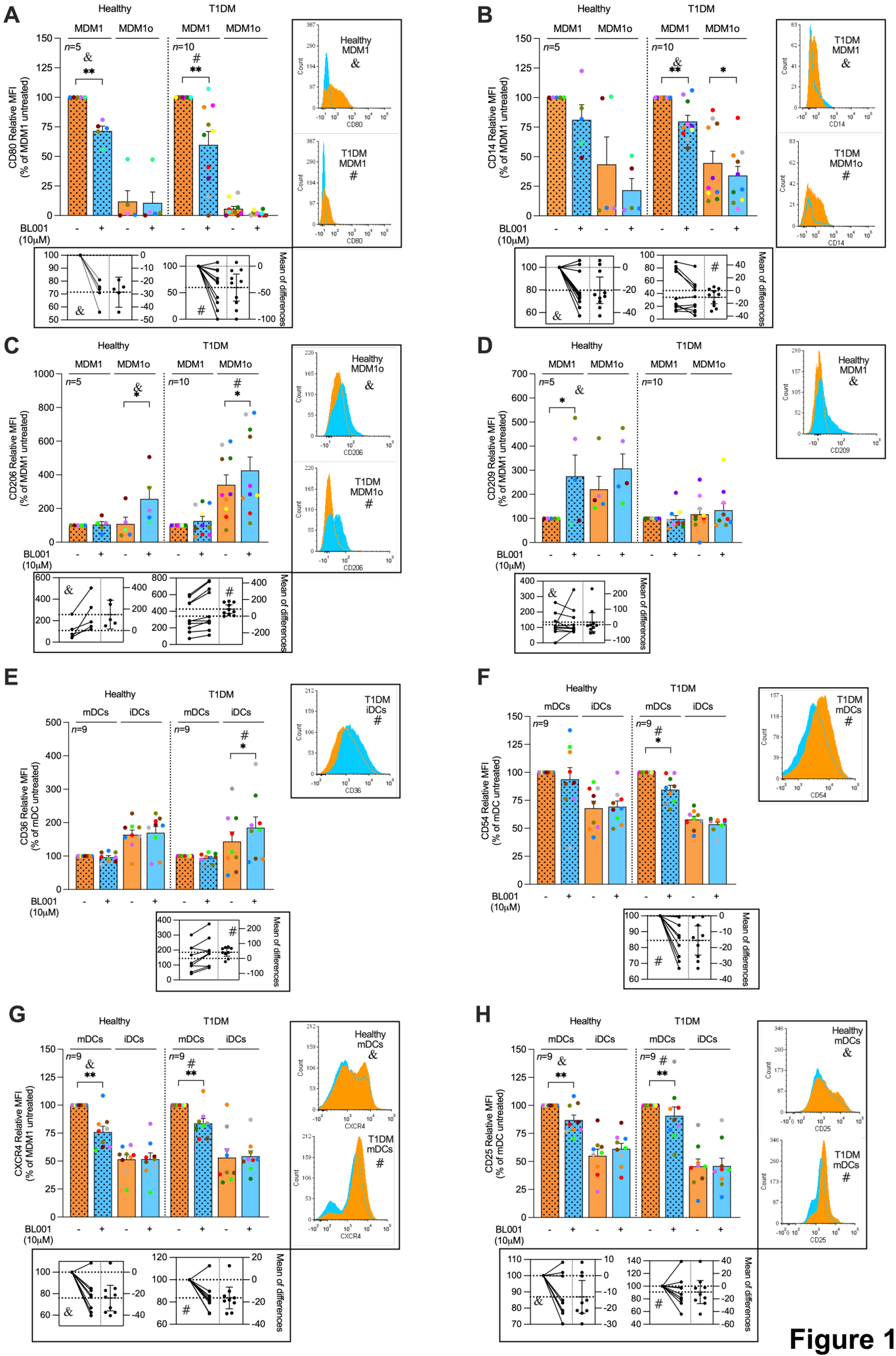
A
Healthy
T1DM
MDM1
MDM1o
CD80 Relative MFI (% of MDM1 untreated)
n=5
n=10
BL001 (10μM)
Healthy MDM1
T1DM MDM1
CD80
Count
Mean of differences
B
CD14 Relative MFI (% of MDM1 untreated)
T1DM MDM1
T1DM MDM1o
CD14
C
CD206 Relative MFI (% of MDM1 untreated)
Healthy MDM1o
T1DM MDM1o
CD206
D
CD209 Relative MFI (% of MDM1 untreated)
Healthy MDM1
CD209
E
mDCs
iDCs
CD36 Relative MFI (% of mDC untreated)
n=9
T1DM iDCs
CD36
F
CD54 Relative MFI (% of mDC untreated)
T1DM mDCs
CD54
G
CXCR4 Relative MFI (% of MDM1 untreated)
Healthy mDCs
T1DM mDCs
CXCR4
H
CD25 Relative MFI (% of mDC untreated)
CD25

Figure 1

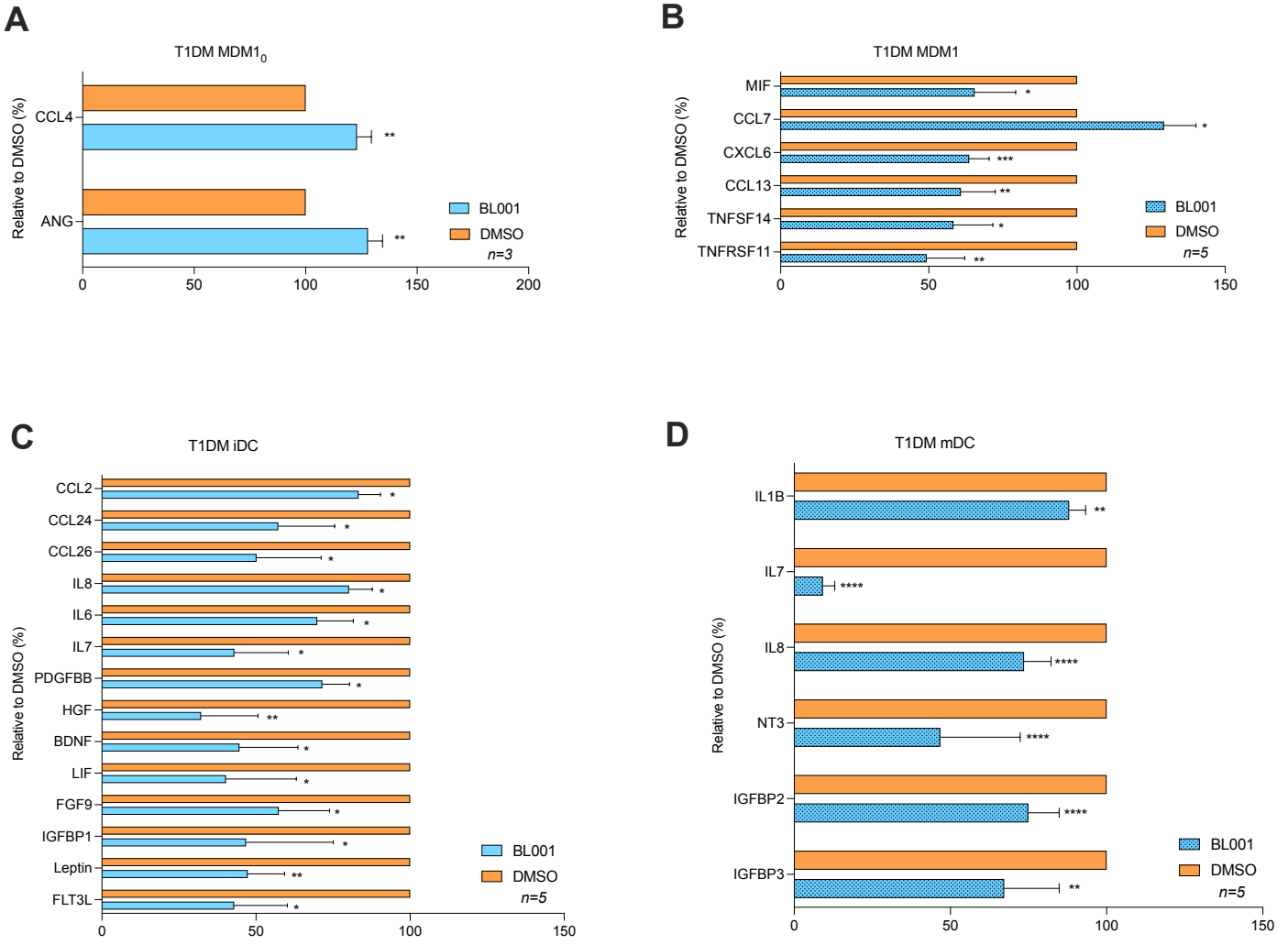
A
T1DM MDM1$_0$
Relative to DMSO (%)
CCL4
ANG
BL001
DMSO
n=3
0
50
100
150
200
B
T1DM MDM1
Relative to DMSO (%)
MIF
CCL7
CXCL6
CCL13
TNFSF14
TNFRSF11
BL001
DMSO
n=5
0
50
100
150
C
T1DM iDC
Relative to DMSO (%)
CCL2
CCL24
CCL26
IL8
IL6
IL7
PDGFBB
HGF
BDNF
LIF
FGF9
IGFBP1
Leptin
FLT3L
BL001
DMSO
n=5
0
50
100
150
D
T1DM mDC
Relative to DMSO (%)
IL1B
IL7
IL8
NT3
IGFBP2
IGFBP3
BL001
DMSO
n=5
0
50
100
150

Figure 2

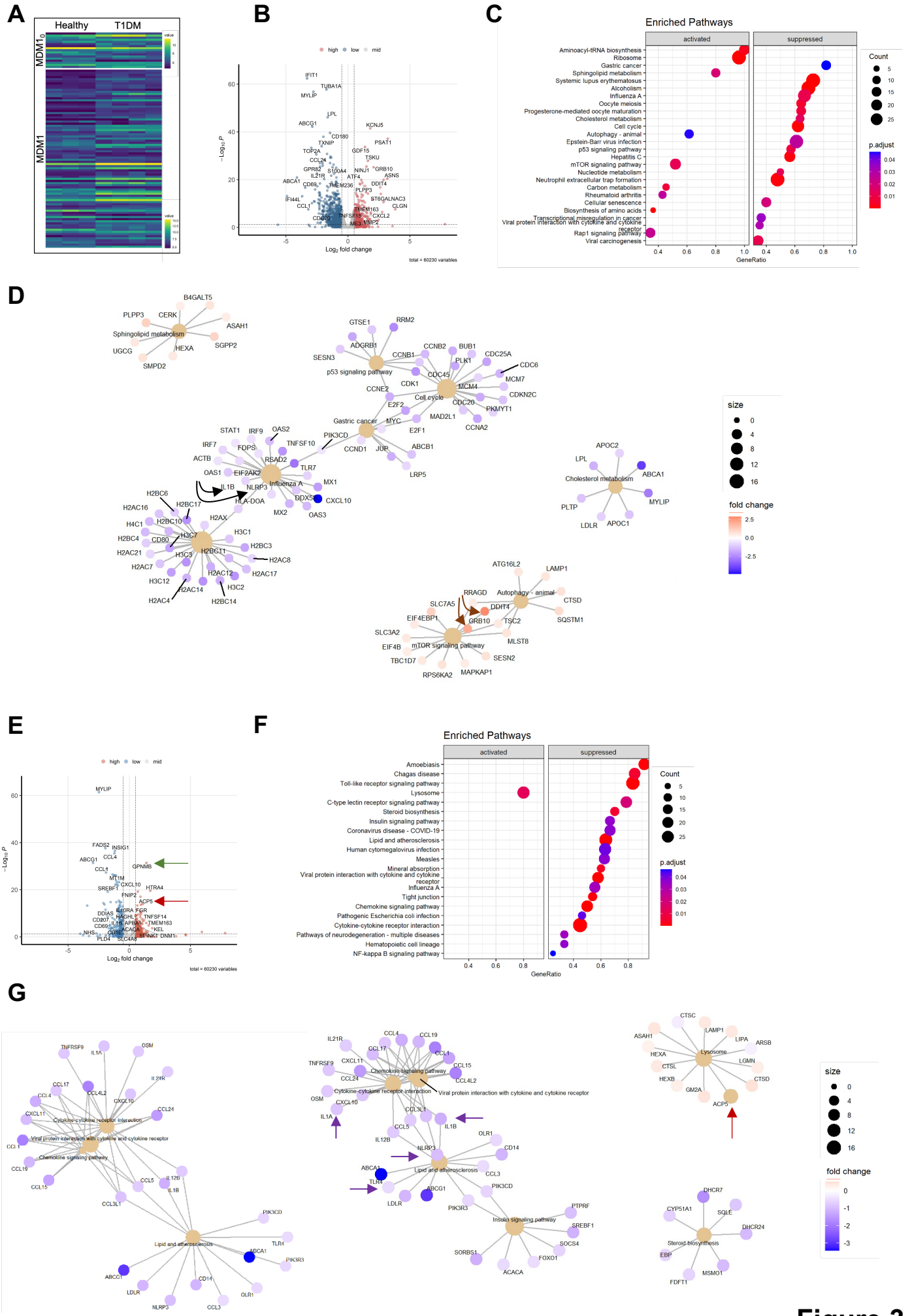
A
Healthy
T1DM
MDM1D
MDM1
B
high
low
mid
$-Log_{10}$ P
Log_2 fold change
total = 60230 variables
C
Enriched Pathways
activated
suppressed
Aminoacyl-tRNA biosynthesis
Ribosome
Gastric cancer
Sphingolipid metabolism
Systemic lupus erythematosus
Alcoholism
Influenza A
Oocyte meiosis
Progesterone-mediated oocyte maturation
Cholesterol metabolism
Cell cycle
Autophagy - animal
Epstein-Barr virus infection
p53 signaling pathway
Hepatitis C
mTOR signaling pathway
Nucleotide metabolism
Neutrophil extracellular trap formation
Carbon metabolism
Rheumatoid arthritis
Cellular senescence
Biosynthesis of amino acids
Transcriptional misregulation in cancer
Viral protein interaction with cytokine and cytokine receptor
Rap1 signaling pathway
Viral carcinogenesis
GeneRatio
Count
p.adjust
D
Sphingolipid metabolism
p53 signaling pathway
Cell cycle
Gastric cancer
Influenza A
Cholesterol metabolism
Autophagy - animal
mTOR signaling pathway
size
fold change
E
high
low
mid
$-Log_{10}$ P
Log_2 fold change
total = 60230 variables
F
Enriched Pathways
activated
suppressed
Amoebiasis
Chagas disease
Toll-like receptor signaling pathway
Lysosome
C-type lectin receptor signaling pathway
Steroid biosynthesis
Insulin signaling pathway
Coronavirus disease - COVID-19
Lipid and atherosclerosis
Human cytomegalovirus infection
Measles
Mineral absorption
Viral protein interaction with cytokine and cytokine receptor
Influenza A
Tight junction
Chemokine signaling pathway
Pathogenic Escherichia coli infection
Cytokine-cytokine receptor interaction
Pathways of neurodegeneration - multiple diseases
Hematopoietic cell lineage
NF-kappa B signaling pathway
GeneRatio
Count
p.adjust
G
Cytokine-cytokine receptor interaction
Viral protein interaction with cytokine and cytokine receptor
Chemokine signaling pathway
Lipid and atherosclerosis
Lysosome
Insulin signaling pathway
Steroid biosynthesis
size
fold change

Figure 3

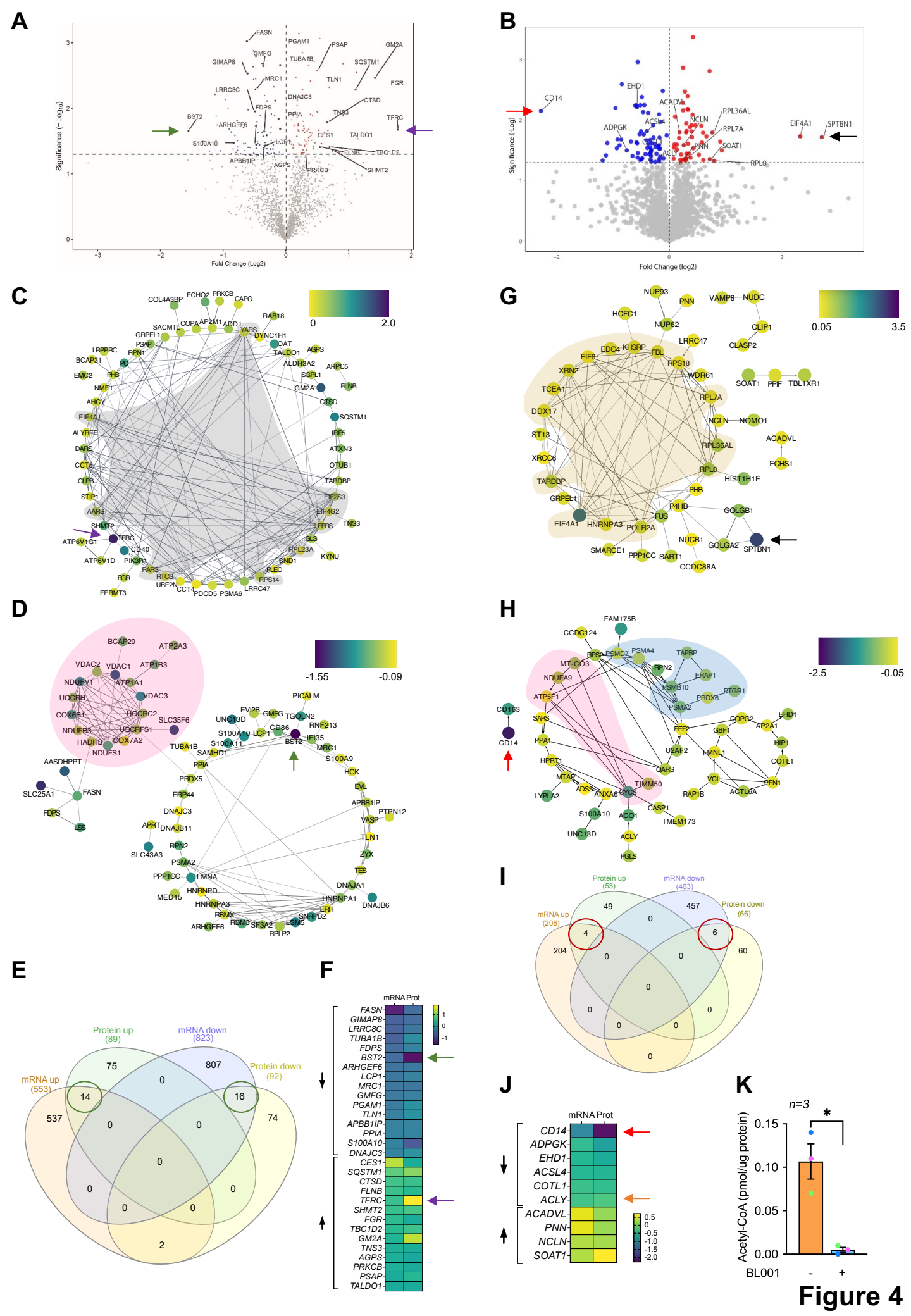
A
Significance (−Log10)
Fold Change (Log2)
FASN
PGAM1
PSAP
GM2A
GMFG
TUBA1B
SQSTM1
GIMAP8
MRC1
TLN1
FGR
LRRC8C
DNAJC3
CTSD
FDPS
PPIA
TNS3
TFRC
BST2
ARHGEF6
CES1
TALDO1
S100A10
LCP1
ELNB
TBC1D2
APBB1IP
AGPS
PRKCB
SHMT2
B
Significance (-Log)
Fold Change (log2)
CD14
EHD1
ACADVL
RPL36AL
ACSL4
NCLN
RPL7A
ADPGK
EIF4A1
SPTBN1
PNN
SOAT1
ACLY
RPL8
C
0
2.0
COL4A3BP
FCHO2
PRKCB
CAPG
RAB18
SACM1L
COPA
AP2M1
ADD1
YARS
GRPEL1
DYNC1H1
PSAP
OAT
LRPPRC
RPN1
TALDO1
AGPS
BCAP31
FC
ALDH3A2
ARPC5
EMC2
PHB
SGPL1
NME1
GM2A
FLNB
AHCY
CTSD
EIF4A1
SQSTM1
ALYREF
IRF5
DARS
ATXN3
CCT6
OTUB1
CLPB
TARDBP
STIP1
EIF2S3
AARS
EIF4G2
SHMT2
EPRS
TNS3
ATP6V1G1
TFRC
GLS
CD40
RPL23A
ATP6V1D
PIK3R1
KYNU
SND1
RARS
PLEC
FGR
RTCB
RPS14
UBE2N
CCT4
PDCD5
PSMA6
LRRC47
FERMT3
G
0.05
3.5
NUP93
PNN
VAMP8
NUDC
HCFC1
NUP62
CLIP1
LRRC47
CLASP2
EDC4
KHSRP
EIF6
FBL
RPS18
XRN2
WDR61
SOAT1
PPIF
TBL1XR1
TCEA1
RPL7A
DDX17
NCLN
NOMO1
ST13
ACADVL
RPL36AL
XRCC6
ECHS1
RPL8
HIST1H1E
TARDBP
PHB
GRPEL1
P4HB
GOLGB1
EIF4A1
HNRNPA3
FUS
POLR2A
NUCB1
GOLGA2
SPTBN1
SMARCE1
PPP1CC
SART1
CCDC88A
D
-1.55
-0.09
BCAP29
ATP2A3
VDAC2
VDAC1
ATP1B3
NDUFV1
ATP1A1
UQCRH
VDAC3
COX6B1
UQCRC2
SLC35F6
NDUFB5
UQCRFS1
HADHB
COX7A2
NDUFS1
AASDHPPT
SLC25A1
FASN
FDPS
LSS
PICALM
EVI2B
GMFG
UNC13D
TGOLN2
CD86
RNF213
S100A10
LCP1
S100A11
BST2
IFI35
TUBA1B
SAMHD1
MRC1
PPIA
S100A9
HCK
PRDX5
EVL
ERP44
APBB1IP
DNAJC3
PTPN12
APRT
DNAJB11
VASP
RPN2
TLN1
SLC43A3
ZYX
PSMA2
TES
PPP1CC
LMNA
DNAJA1
HNRNPD
MED15
HNRNPA1
DNAJB6
HNRNPA3
EPH
RBMX
SNRPB2
ARHGEF6
RBM3
SF3A2
LSM5
RPLP2
E
Protein up
(89)
mRNA down
(823)
mRNA up
(553)
Protein down
(92)
75
807
14
16
537
74
0
0
0
0
0
0
0
0
2
F
mRNA Prot
1
0
-1
FASN
GIMAP8
LRRC8C
TUBA1B
FDPS
BST2
ARHGEF6
LCP1
MRC1
GMFG
PGAM1
TLN1
APBB1IP
PPIA
S100A10
DNAJC3
CES1
SQSTM1
CTSD
FLNB
TFRC
SHMT2
FGR
TBC1D2
GM2A
TNS3
AGPS
PRKCB
PSAP
TALDO1
G
0.05
3.5
H
-2.5
-0.05
FAM175B
CCDC124
RPS2
PSMD2
PSMA4
TAPBP
MT-CO3
RPN2
ERAP1
NDUFA9
PSMB10
PTGR1
ATP5F1
PRDX6
PSMA2
CD163
SARS
COPG2
EHD1
EEF2
GBF1
AP2A1
CD14
PPA1
HIP1
U2AF2
FMNL1
COTL1
HPRT1
CARS
MTAP
VCL
PFN1
TIMM50
ADSS
ANXA6
CYCS
ACTL6A
LYPLA2
RAP1B
CASP1
S100A10
ACO1
TMEM173
UNC13D
ACLY
PGLS
I
Protein up
(53)
mRNA down
(463)
mRNA up
(208)
Protein down
(66)
49
457
4
6
204
60
0
0
0
0
0
0
0
0
0
J
mRNA Prot
CD14
ADPGK
EHD1
ACSL4
COTL1
ACLY
ACADVL
PNN
NCLN
SOAT1
0.5
0
-0.5
-1.0
-1.5
-2.0
K
n=3
*
Acetyl-CoA (pmol/ug protein)
0.15
0.10
0.05
0.00
BL001
-
+

Figure 4

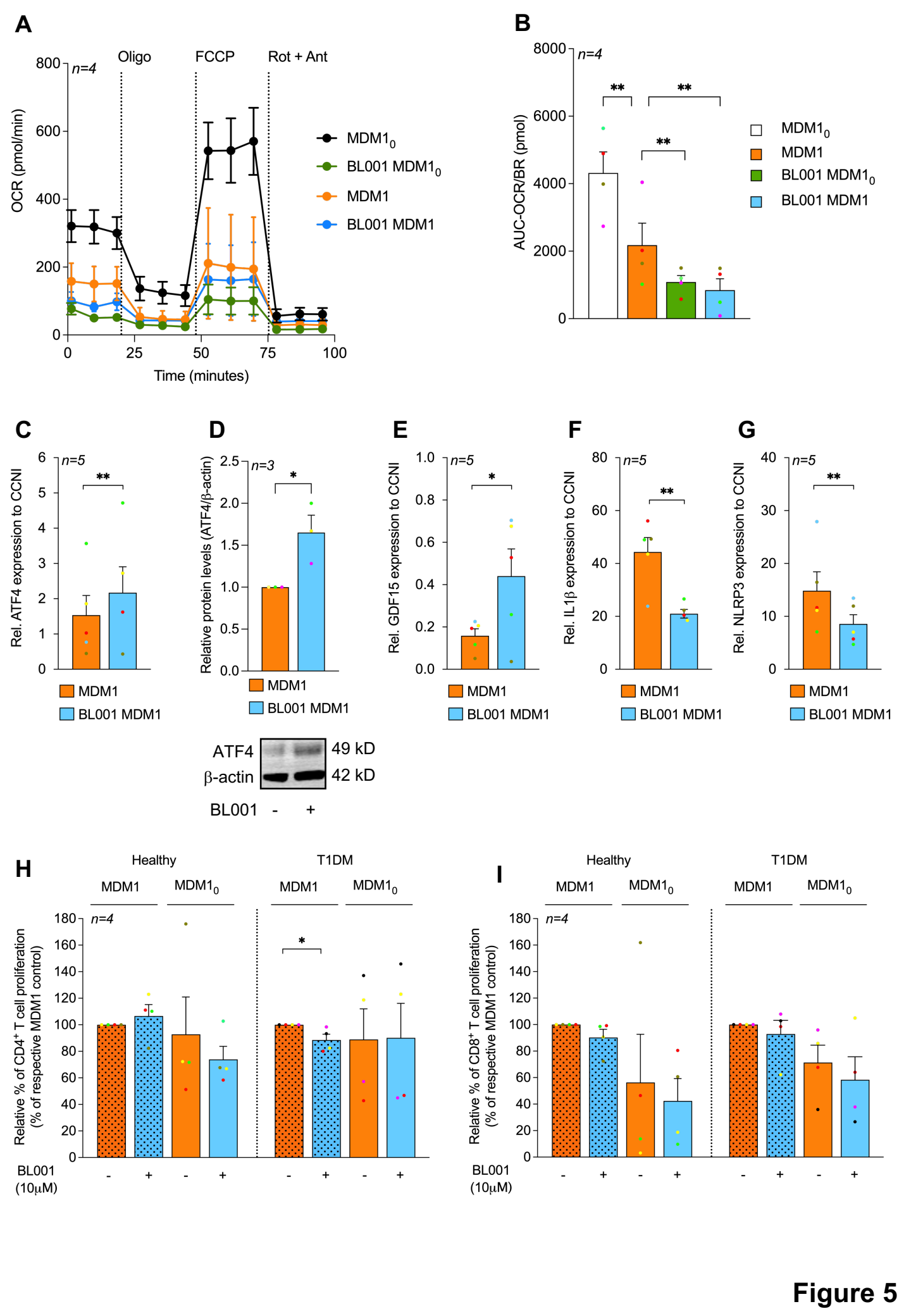
A
n=4
Oligo
FCCP
Rot + Ant
OCR (pmol/min)
Time (minutes)
MDM1$_0$
BL001 MDM1$_0$
MDM1
BL001 MDM1
B
n=4
AUC-OCR/BR (pmol)
C
n=5
Rel. ATF4 expression to CCNI
D
n=3
Relative protein levels (ATF4/β-actin)
ATF4
β-actin
49 kD
42 kD
BL001 - +
E
n=5
Rel. GDF15 expression to CCNI
F
n=5
Rel. IL1β expression to CCNI
G
n=5
Rel. NLRP3 expression to CCNI
H
Healthy
T1DM
MDM1
MDM1$_0$
n=4
Relative % of CD4$^+$ T cell proliferation (% of respective MDM1 control)
BL001 (10μM)
I
Relative % of CD8$^+$ T cell proliferation (% of respective MDM1 control)

Figure 5

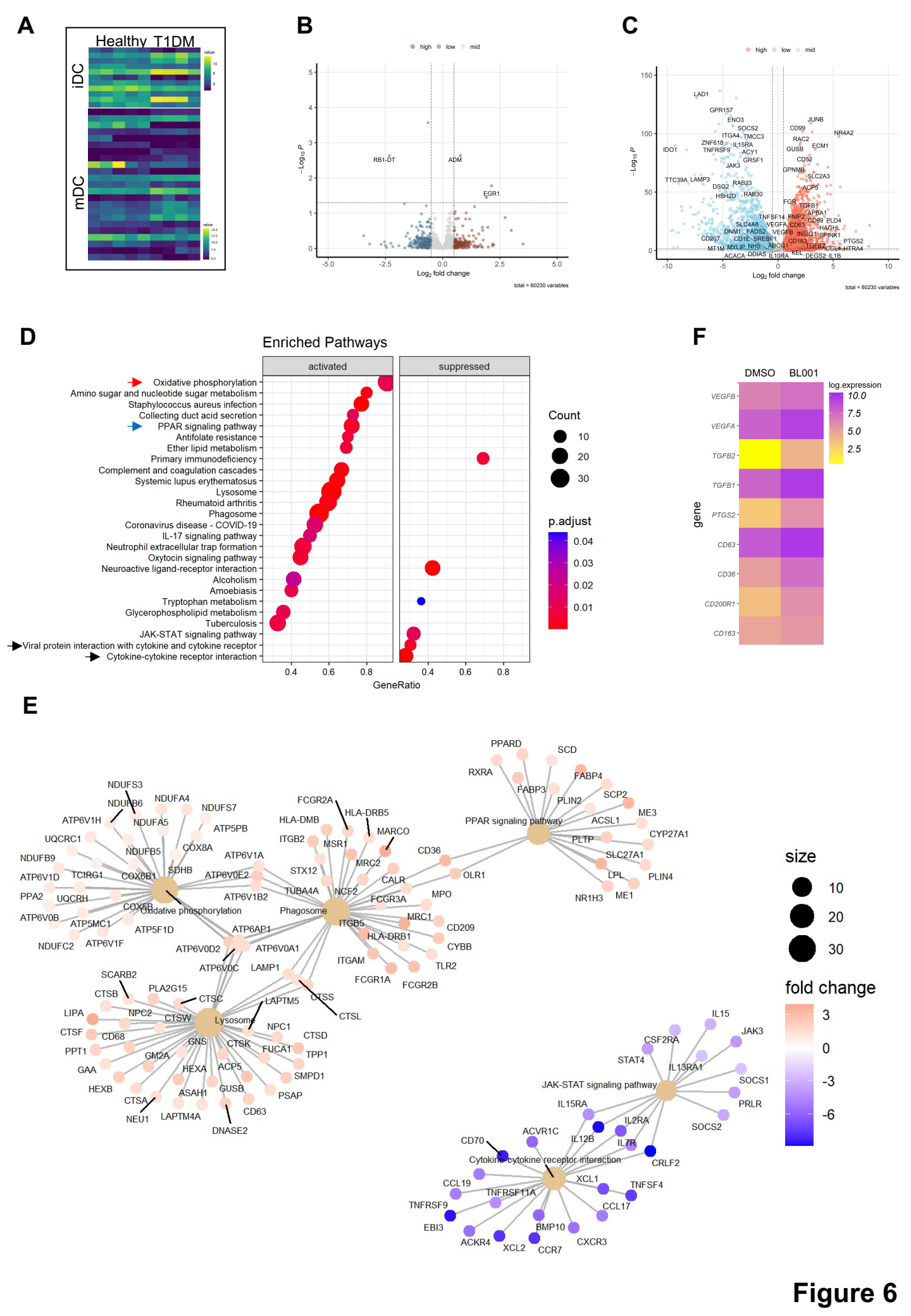
A
Healthy T1DM
iDC
mDC
B
high
low
mid
RB1-DT
ADM
EGR1
Log2 fold change
total = 60230 variables
C
LAD1
GPR157
ENO3
SOCS2
ITGA4
TMCC3
ZNF618
IL15RA
TNFRSF9
ACY1
GRSF1
JAK3
IDO1
TTC39A
LAMP3
DSG2
RAB23
HSH2D
RAB30
JUNB
CD99
NR4A2
RAC2
GUSB
ECM1
CD52
GPNMB
SLC2A3
ACP5
FGR
TGFB1
APBA1
TNFSF14
FNIP2
CD69
PLD4
SLC4A8
VEGFA
CD63
HAGHL
DNM1
FADS2
VEGFB
INSIG1
SPINK1
CD207
CD1E
SREBF1
CD163
PTGS2
MT1M
MYLIP
NHS
ABCG1
TGFB2
CCL4
HTRA4
ACACA
DDIAS
IL10RA
KEL
DEGS2
IL1B
Log2 fold change
total = 60230 variables
D
Enriched Pathways
activated
suppressed
Oxidative phosphorylation
Amino sugar and nucleotide sugar metabolism
Staphylococcus aureus infection
Collecting duct acid secretion
PPAR signaling pathway
Antifolate resistance
Ether lipid metabolism
Primary immunodeficiency
Complement and coagulation cascades
Systemic lupus erythematosus
Lysosome
Rheumatoid arthritis
Phagosome
Coronavirus disease - COVID-19
IL-17 signaling pathway
Neutrophil extracellular trap formation
Oxytocin signaling pathway
Neuroactive ligand-receptor interaction
Alcoholism
Amoebiasis
Tryptophan metabolism
Glycerophospholipid metabolism
Tuberculosis
JAK-STAT signaling pathway
Viral protein interaction with cytokine and cytokine receptor
Cytokine-cytokine receptor interaction
GeneRatio
Count
10
20
30
p.adjust
0.04
0.03
0.02
0.01
F
DMSO
BL001
log.expression
10.0
7.5
5.0
2.5
gene
VEGFB
VEGFA
TGFB2
TGFB1
PTGS2
CD63
CD36
CD200R1
CD163
E
PPARD
SCD
RXRA
FABP4
FABP3
PLIN2
SCP2
PPAR signaling pathway
ACSL1
ME3
PLTP
CYP27A1
SLC27A1
LPL
PLIN4
NR1H3
ME1
NDUFS3
NDUFB6
NDUFA4
NDUFS7
ATP6V1H
NDUFA5
ATP5PB
UQCRC1
NDUFB5
COX8A
NDUFB9
ATP6V1A
ATP6V1D
TCIRG1
COX6B1
SDHB
ATP6V0E2
PPA2
UQCRH
ATP6V1B2
ATP6V0B
COX5B
Oxidative phosphorylation
ATP5MC1
ATP5F1D
NDUFC2
ATP6V1F
ATP6AP1
ATP6V0D2
ATP6V0A1
ATP6V0C
LAMP1
FCGR2A
HLA-DRB5
HLA-DMB
MARCO
ITGB2
MSR1
CD36
MRC2
STX12
OLR1
CALR
TUBA4A
NCF2
FCGR3A
MPO
Phagosome
ITGB5
MRC1
CD209
HLA-DRB1
CYBB
ITGAM
TLR2
FCGR1A
FCGR2B
SCARB2
CTSB
PLA2G15
CTSC
CTSS
LAPTM5
CTSL
LIPA
NPC2
CTSW
Lysosome
NPC1
CTSF
CD68
CTSD
PPT1
GNS
CTSK
FUCA1
TPP1
GM2A
GAA
HEXA
ACP5
SMPD1
HEXB
ASAH1
GUSB
PSAP
CTSA
NEU1
LAPTM4A
CD63
DNASE2
size
10
20
30
fold change
3
0
-3
-6
IL15
JAK3
CSF2RA
STAT4
IL13RA1
SOCS1
JAK-STAT signaling pathway
PRLR
IL15RA
IL2RA
SOCS2
ACVR1C
IL12B
IL7R
CD70
CRLF2
Cytokine-cytokine receptor interaction
XCL1
CCL19
TNFSF4
TNFRSF11A
CCL17
TNFRSF9
EBI3
BMP10
ACKR4
XCL2
CCR7
CXCR3

Figure 6

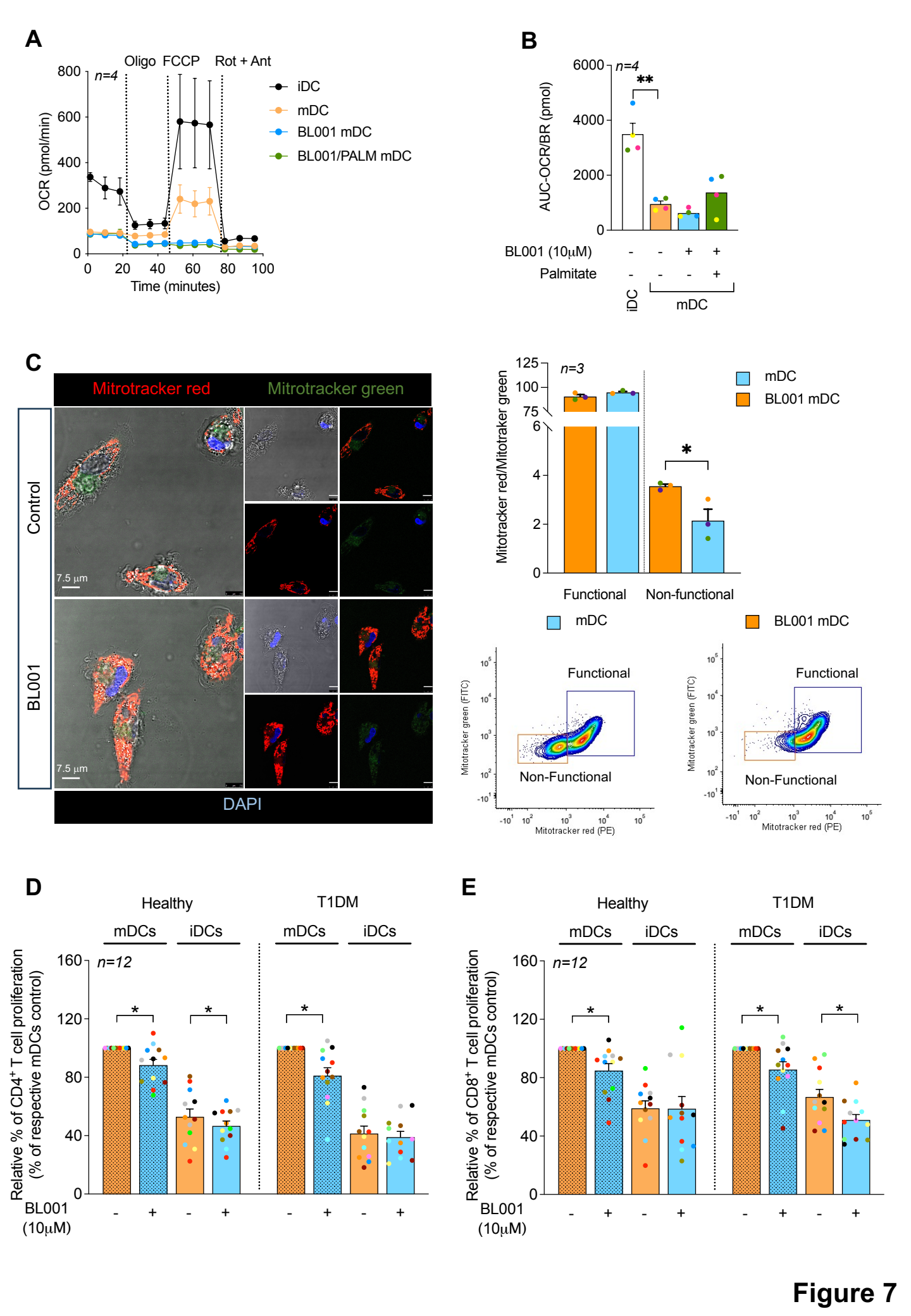
A
Oligo
FCCP
Rot + Ant
n=4
OCR (pmol/min)
Time (minutes)
iDC
mDC
BL001 mDC
BL001/PALM mDC
B
n=4
AUC-OCR/BR (pmol)
BL001 (10μM)
Palmitate
iDC
mDC
C
Mitrotracker red
Mitrotracker green
Control
BL001
7.5 μm
DAPI
n=3
Mitotracker red/Mitotraker green
mDC
BL001 mDC
Functional
Non-functional
Functional
Non-Functional
Mitotracker green (FITC)
Mitotracker red (PE)
D
Healthy
T1DM
mDCs
iDCs
n=12
Relative % of CD4+ T cell proliferation (% of respective mDCs control)
BL001 (10μM)
E
Relative % of CD8+ T cell proliferation (% of respective mDCs control)

Figure 7

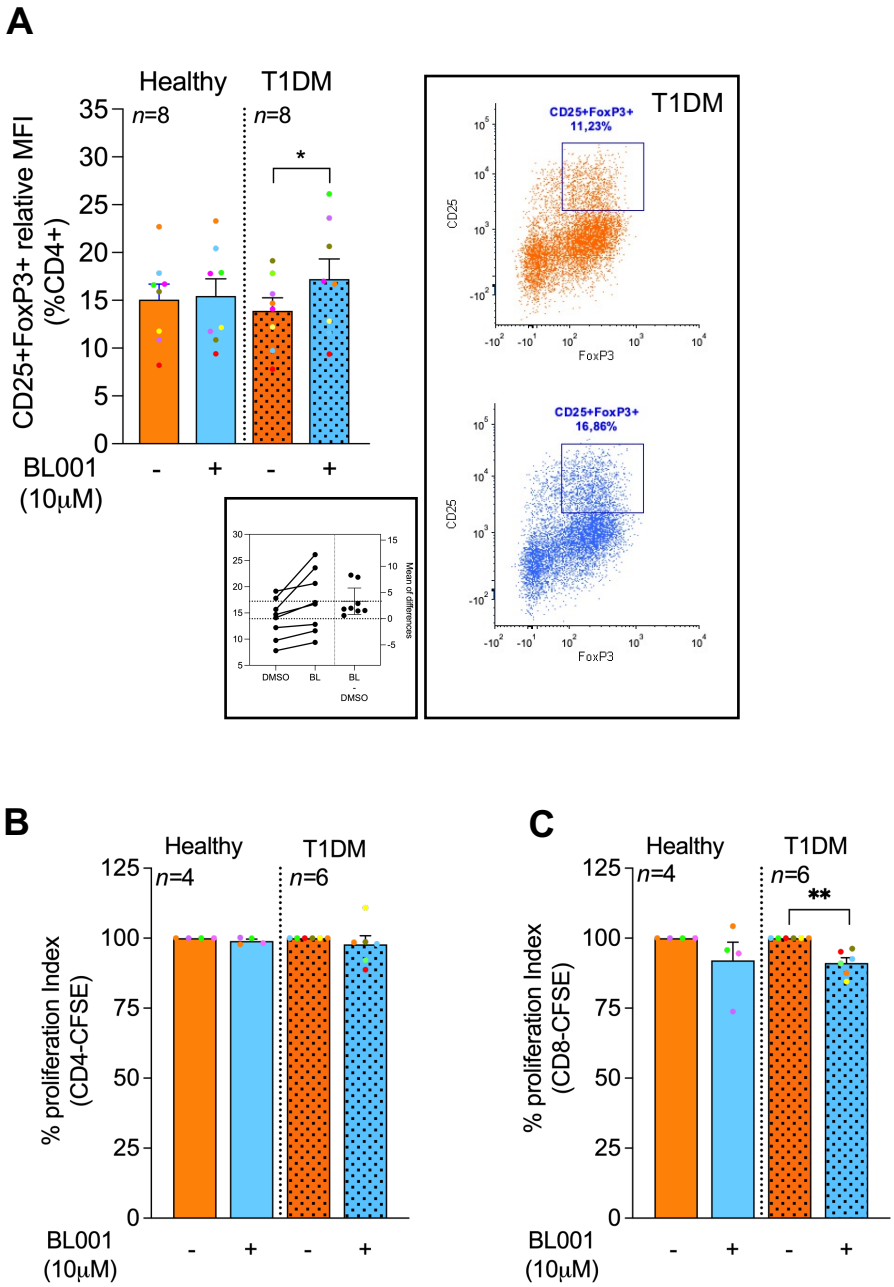
A
Healthy
T1DM
n=8
n=8
*
CD25+FoxP3+ relative MFI (%CD4+)
BL001 (10μM)
- + - +
T1DM
CD25+FoxP3+ 11,23%
CD25+FoxP3+ 16,86%
CD25
FoxP3
DMSO
BL
Mean of differences
B
Healthy
T1DM
n=4
n=6
% proliferation Index (CD4-CFSE)
C
**
% proliferation Index (CD8-CFSE)

Figure 8

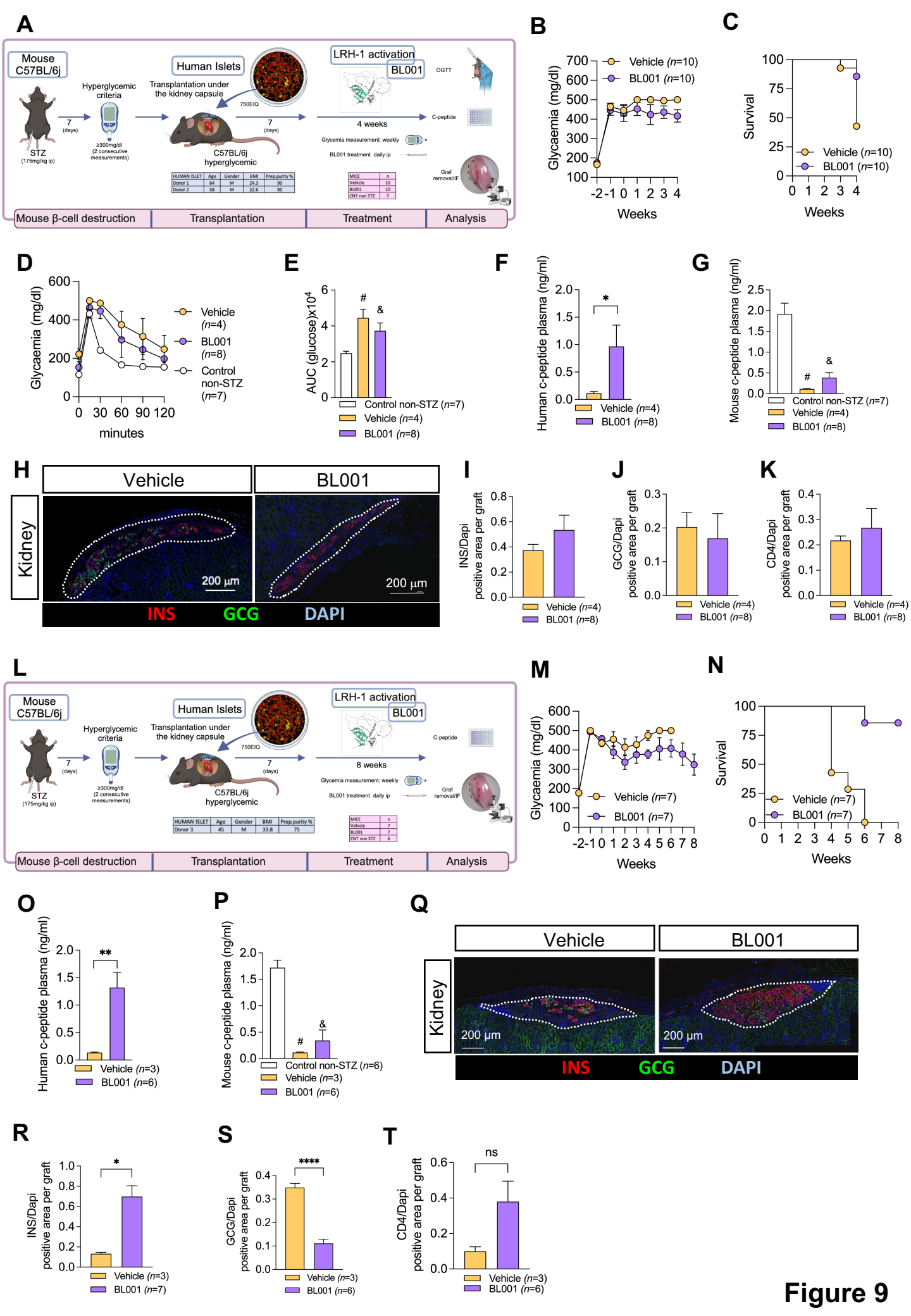
A
Mouse C57BL/6j
STZ (175mg/kg ip)
7 (days)
Hyperglycemic criteria
≥300mg/dl (2 consecutive measurements)
Human Islets
Transplantation under the kidney capsule
750EIQ
C57BL/6j hyperglycemic
7 (days)
LRH-1 activation
BL001
4 weeks
OGTT
C-peptide
Glycemia measurement: weekly
BL001 treatment daily ip
Graf removal/IF
Mouse β-cell destruction
Transplantation
Treatment
Analysis
B
Glycaemia (mg/dl)
Weeks
Vehicle (n=10)
BL001 (n=10)
C
Survival
Weeks
Vehicle (n=10)
BL001 (n=10)
D
Glycaemia (mg/dl)
minutes
Vehicle (n=4)
BL001 (n=8)
Control non-STZ (n=7)
E
AUC (glucose)x10^4
Control non-STZ (n=7)
Vehicle (n=4)
BL001 (n=8)
F
Human c-peptide plasma (ng/ml)
Vehicle (n=4)
BL001 (n=8)
G
Mouse c-peptide plasma (ng/ml)
Control non-STZ (n=7)
Vehicle (n=4)
BL001 (n=8)
H
Vehicle
BL001
Kidney
200 µm
INS
GCG
DAPI
I
INS/Dapi positive area per graft
Vehicle (n=4)
BL001 (n=8)
J
GCG/Dapi positive area per graft
Vehicle (n=4)
BL001 (n=8)
K
CD4/Dapi positive area per graft
Vehicle (n=4)
BL001 (n=8)
L
Mouse C57BL/6j
STZ (175mg/kg ip)
7 (days)
Hyperglycemic criteria
≥300mg/dl (2 consecutive measurements)
Human Islets
Transplantation under the kidney capsule
750EIQ
C57BL/6j hyperglycemic
7 (days)
LRH-1 activation
BL001
8 weeks
C-peptide
Glycemia measurement: weekly
BL001 treatment daily ip
Graf removal/IF
Mouse β-cell destruction
Transplantation
Treatment
Analysis
M
Glycaemia (mg/dl)
Weeks
Vehicle (n=7)
BL001 (n=7)
N
Survival
Weeks
Vehicle (n=7)
BL001 (n=7)
O
Human c-peptide plasma (ng/ml)
Vehicle (n=3)
BL001 (n=6)
P
Mouse c-peptide plasma (ng/ml)
Control non-STZ (n=6)
Vehicle (n=3)
BL001 (n=6)
Q
Vehicle
BL001
Kidney
200 µm
INS
GCG
DAPI
R
INS/Dapi positive area per graft
Vehicle (n=3)
BL001 (n=7)
S
GCG/Dapi positive area per graft
Vehicle (n=3)
BL001 (n=6)
T
CD4/Dapi positive area per graft
Vehicle (n=3)
BL001 (n=6)

Figure 9

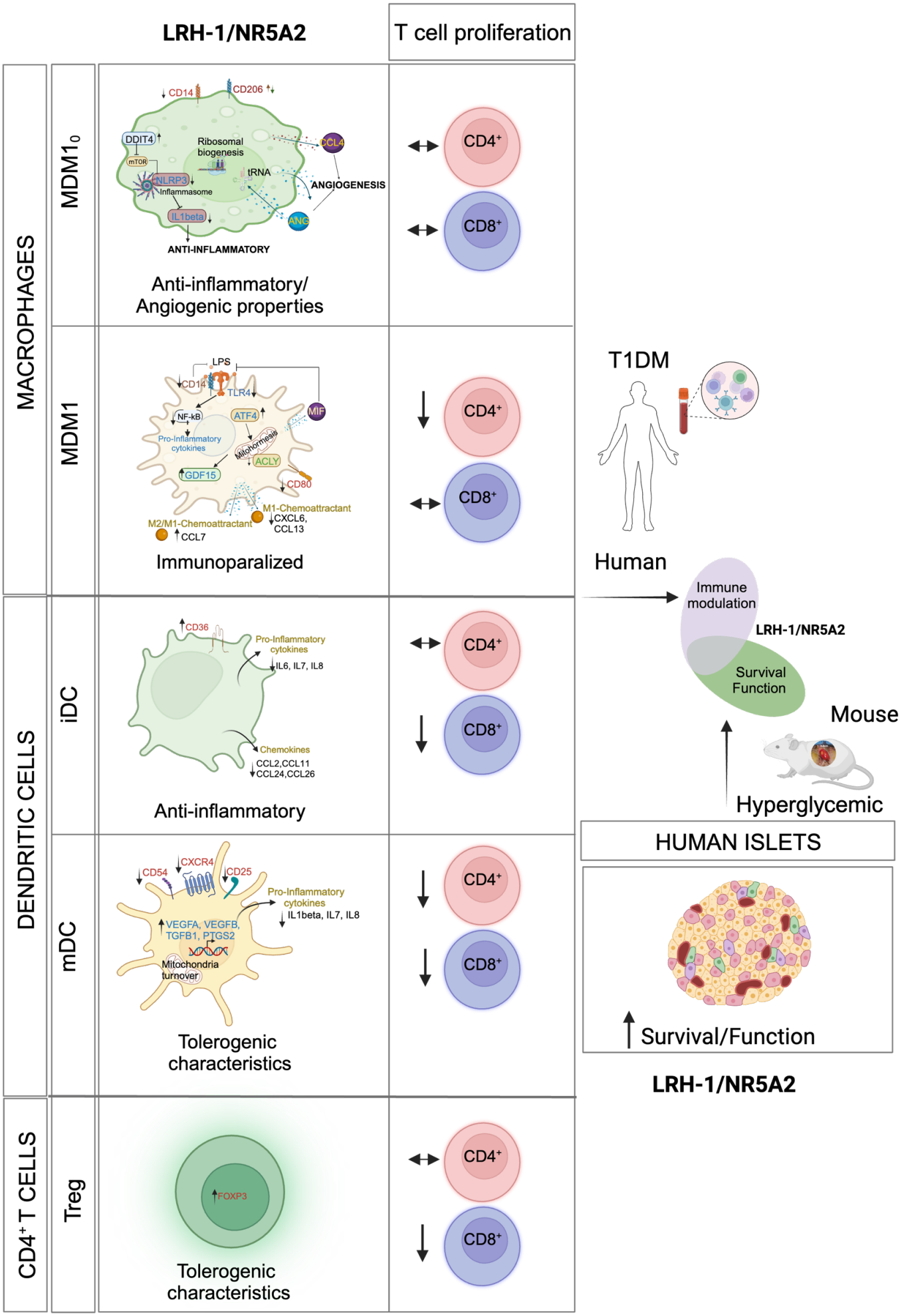
LRH-1/NR5A2
T cell proliferation
MACROPHAGES
MDM1₀
CD14
CD206
DDIT4
mTOR
Ribosomal biogenesis
CCL4
NLRP3
Inflammasome
tRNA
ANGIOGENESIS
IL1beta
ANG
ANTI-INFLAMMATORY
Anti-inflammatory/ Angiogenic properties
CD4+
CD8+
MDM1
LPS
CD14
TLR4
MIF
NF-kB
ATF4
Pro-Inflammatory cytokines
Mitohormesis
ACLY
GDF15
CD80
M1-Chemoattractant
CXCL6, CCL13
M2/M1-Chemoattractant
CCL7
Immunoparalized
DENDRITIC CELLS
iDC
CD36
Pro-Inflammatory cytokines
IL6, IL7, IL8
Chemokines
CCL2,CCL11
CCL24,CCL26
Anti-inflammatory
mDC
CD54
CXCR4
CD25
Pro-Inflammatory cytokines
IL1beta, IL7, IL8
VEGFA, VEGFB, TGFB1, PTGS2
Mitochondria turnover
Tolerogenic characteristics
CD4+ T CELLS
Treg
FOXP3
Tolerogenic characteristics
T1DM
Human
Immune modulation
LRH-1/NR5A2
Survival Function
Mouse
Hyperglycemic
HUMAN ISLETS
Survival/Function
LRH-1/NR5A2

Figure 10

Table 1: Characteristics and clinical data of blood donors. Samples were collected from three independent National Hospitals. N/A, not applicable.

	Healthy subjects	Individuals with T1DM
N	37	68
Gender (F/M)	20F / 17M	32F / 36M
Age (years)	33 ± 9	37 ± 10
BMI (kg/m^2)	23 ± 3	24 ± 4
Age at diagnosis (years)	N/A	20 ± 12
Progression (years)	N/A	16 ± 11
HbA1c (%)	N/A	7,0 ± 0,9
Insulin dose (IU/kg/day)	N/A	0,53 ± 0,17